

NASA-CR-170,109

NASA-CR-170109
19830013407

AEROSPACE REPORT NO.
ATR-83(7951)-2

Mirror Instability and the Origin of Morningside Auroral Structure

Prepared by
Y. T. CHIU, M. SCHULZ, J. F. FENNELL,
and A. M. KISHI
Space Sciences Laboratory

1 March 1983

LIBRARY COPY

MAR 8 - 1983

LANGLEY RESEARCH CENTER
LIBRARY, NASA
HAMPTON, VIRGINIA

Prepared for
NATIONAL AERONAUTICS AND SPACE ADMINISTRATION
Headquarters, Washington, D.C. 20545

Contract No. NASW-3434



Laboratory Operations

THE AEROSPACE CORPORATION



NF02582

All Blank Pages
Intentionally Left Blank
To Keep Document Continuity

LABORATORY OPERATIONS

The Laboratory Operations of The Aerospace Corporation is conducting experimental and theoretical investigations necessary for the evaluation and application of scientific advances to new military space systems. Versatility and flexibility have been developed to a high degree by the laboratory personnel in dealing with the many problems encountered in the nation's rapidly developing space systems. Expertise in the latest scientific developments is vital to the accomplishment of tasks related to these problems. The laboratories that contribute to this research are:

Aerophysics Laboratory: Launch vehicle and reentry aerodynamics and heat transfer, propulsion chemistry and fluid mechanics, structural mechanics, flight dynamics; high-temperature thermomechanics, gas kinetics and radiation; research in environmental chemistry and contamination; cw and pulsed chemical laser development including chemical kinetics, spectroscopy, optical resonators and beam pointing, atmospheric propagation, laser effects and countermeasures.

Chemistry and Physics Laboratory: Atmospheric chemical reactions, atmospheric optics, light scattering, state-specific chemical reactions and radiation transport in rocket plumes, applied laser spectroscopy, laser chemistry, battery electrochemistry, space vacuum and radiation effects on materials, lubrication and surface phenomena, thermionic emission, photosensitive materials and detectors, atomic frequency standards, and bioenvironmental research and monitoring.

Electronics Research Laboratory: Microelectronics, GaAs low-noise and power devices, semiconductor lasers, electromagnetic and optical propagation phenomena, quantum electronics, laser communications, lidar, and electro-optics; communication sciences, applied electronics, semiconductor crystal and device physics, radiometric imaging; millimeter-wave and microwave technology.

Information Sciences Research Office: Program verification, program translation, performance-sensitive system design, distributed architectures for spaceborne computers, fault-tolerant computer systems, artificial intelligence, and microelectronics applications.

Materials Sciences Laboratory: Development of new materials: metal matrix composites, polymers, and new forms of carbon; component failure analysis and reliability; fracture mechanics and stress corrosion; evaluation of materials in space environment; materials performance in space transportation systems; analysis of systems vulnerability and survivability in enemy-induced environments.

Space Sciences Laboratory: Atmospheric and ionospheric physics, radiation from the atmosphere, density and composition of the upper atmosphere, aurorae and airglow; magnetospheric physics, cosmic rays, generation and propagation of plasma waves in the magnetosphere; solar physics, infrared astronomy; the effects of nuclear explosions, magnetic storms, and solar activity on the earth's atmosphere, ionosphere, and magnetosphere; the effects of optical, electromagnetic, and particulate radiations in space on space systems.

. . .

Aerospace Report No.
ATR-83(7951)-2

MIRROR INSTABILITY AND THE ORIGIN OF
MORNINGSIDE AURORAL STRUCTURE

Prepared by
Y. T. Chiu, M. Schulz, J. F. Fennell, and A. M. Kishi
Space Sciences Laboratory

1 March 1983

Laboratory Operations
THE AEROSPACE CORPORATION
El Segundo, Calif. 90245

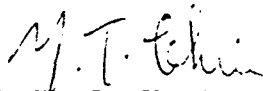
Contract No. NASW-3434

Prepared for
NATIONAL AERONAUTICS AND SPACE ADMINISTRATION
Headquarters, Washington, D.C. 20545

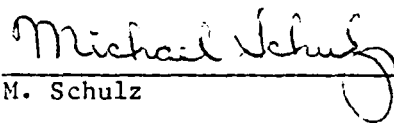
N83-21678#

MIRROR INSTABILITY AND THE ORIGIN OF
MORNINGSIDE AURORAL STRUCTURE

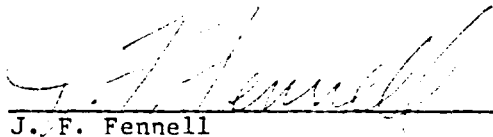
Prepared



Y. T. Chiu



M. Schulz

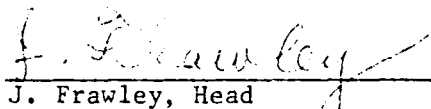


J. F. Fennell

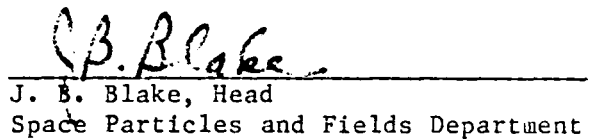


A. M. Kishi

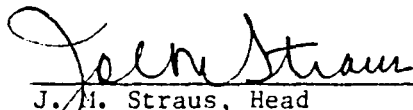
Approved



J. Frawley, Head
Mathematics and Analysis Department



J. B. Blake, Head
Space Particles and Fields Department



J. M. Straus, Head
Atmospheric Sciences Department



H. R. Rugge, Director
Space Sciences Laboratory

Abstract

Auroral optical imagery shows marked differences between auroral features of the evening and morning sectors: the separation between diffuse and discrete auroras in the evening sector is not distinct in the morning sector, which is dominated by auroral patches and multiple banded structures aligned along some direction. Plasma distribution function signatures also show marked differences: downward electron beams and inverted-V signatures prefer the evening sector, while the electron spectra on the morning sector are similar to the diffuse aurora. We have constructed a theory of morningside auroras consistent with these features. The theory is based on modulation of the growth rates of electron cyclotron waves by the mirror instability, which is in turn driven by inward-convected ions that have become anisotropic. This modulation produces alternating bands of enhanced and reduced electron precipitation which approximate the observed multiple auroral bands and patches of the morning sector.

Acknowledgments

It is a pleasure to learn about morningside auroral morphology from S.

-I. Akasofu, D. S. Evans, J. R. Kan, and R. R. Vondrak.

CONTENTS

ABSTRACT.....	v
ACKNOWLEDGMENTS.....	vi
I. INTRODUCTION.....	1
II. MORNINGSIDE AURORAS.....	7
III. FORMATION OF PLASMA DISTRIBUTIONS.....	15
IV. MIRROR INSTABILITY AND PLASMA CONVECTION.....	29
V. SELECTION OF \vec{k} VECTOR.....	35
VI. MODULATION OF CYCLOTRON INSTABILITY.....	45
VII. CONCLUSIONS.....	57
REFERENCES.....	59

FIGURES

1.	A schematic illustration of magnetospheric structure showing solid closed and open field lines and their separatrixes L^*	2
2.	Auroral morphology.....	8
3.	Typical electron energy spectra measured by the S3-3 satellite in the evening and morning sectors.....	9
4.	Energy-time spectra of a dawn-dusk pass of the S3-3 satellite.....	11
5a.	Typical dominantly field-perpendicular ion distribution measured by the SCATHA satellite.....	16
5b.	Typical dominantly field-aligned ion distribution measured by the SCATHA satellite.....	17
6.	Typical electron distribution measured by the SCATHA satellite.....	18
7.	Local-time dependence of the transition energy between field-aligned and field-perpendicular populations such as shown in Figs. 5a and 5b.....	20
8.	Equipotential contours (in kV) of a simple convection electric field model according to Eq. (1).....	23
9.	Simple Maxwellian ion distributions mapped from $L = 13$ to (a) $L = 7$ and dawn, and (b) $L = 7$ and dusk.....	26
10.	Dependence of the mirror instability indicator at $L = 9$ [left-hand side of the inequality (11)] on the ion anisotropy T_{\parallel}/T_{\perp} of the discrete aurora.....	33
11.	Contours of constant shear s [defined in Eq. (19)] of the convection flow corresponding to the electric potential of Fig. 8.....	41
12.	Coordinate system used in considering electron flux modulation.....	48

13. Electron flux modulation by mirror instability for the case in which electrostatic cyclotron waves drift with energetic electrons (Model A).....	51
14. Electron flux modulation by mirror instability for the case in which electrostatic cyclotron waves drift with cold plasma (Model B).....	53

I. INTRODUCTION

A major advance in the understanding of auroral arc formation processes in the evening sector has been achieved in the past few years by satellite observations and theoretical interpretations of auroral plasmas and fields [see, for example, Akasofu and Kan, 1981; Mozer et al., 1980; Fennell et al., 1981; Chiu et al., 1982; and references therein]. In particular, the electrodynamic coupling between hot magnetospheric and cold ionospheric plasmas gives rise to a magnetic field-aligned electric potential drop which accelerates electrons downward to form the inverted-V and arc structures. While obviously a great deal of observational and theoretical details need to be examined further, an outline of a theoretical understanding of the relationship between kinetic plasma processes and the global structure of magnetospheric and ionospheric plasmas and electric fields, which define the scale of the evening arcs, has begun to take shape [Chiu et al., 1979; Lyons, 1980, 1981; Chiu and Cornwall, 1981; Chiu et al., 1981a, b; Schulz et al., 1981]. The essential feature of this line of thought is schematically illustrated in Figure 1 [Chiu et al., 1979]. The discrete-auroral oval seems to be a mapping (along magnetic-field lines) of a boundary layer at (or just inside) the magnetospheric surface. The magnetospheric surface consists of the magnetopause and "neutral" sheet. The cross-magnetospheric "convection" electric field necessarily undergoes a sharp reversal (a near-discontinuity) in its meridional component in this boundary layer and across magnetic-field lines that map to the boundary layer. Note the electric field signatures on the separatrices between closed and open magnetic field regimes in Fig. 1. The cold collisional ionospheric plasma near the foot of the auroral flux tube is unable to support such a near-discontinuity in the normal (to \vec{B}) component of an elec-

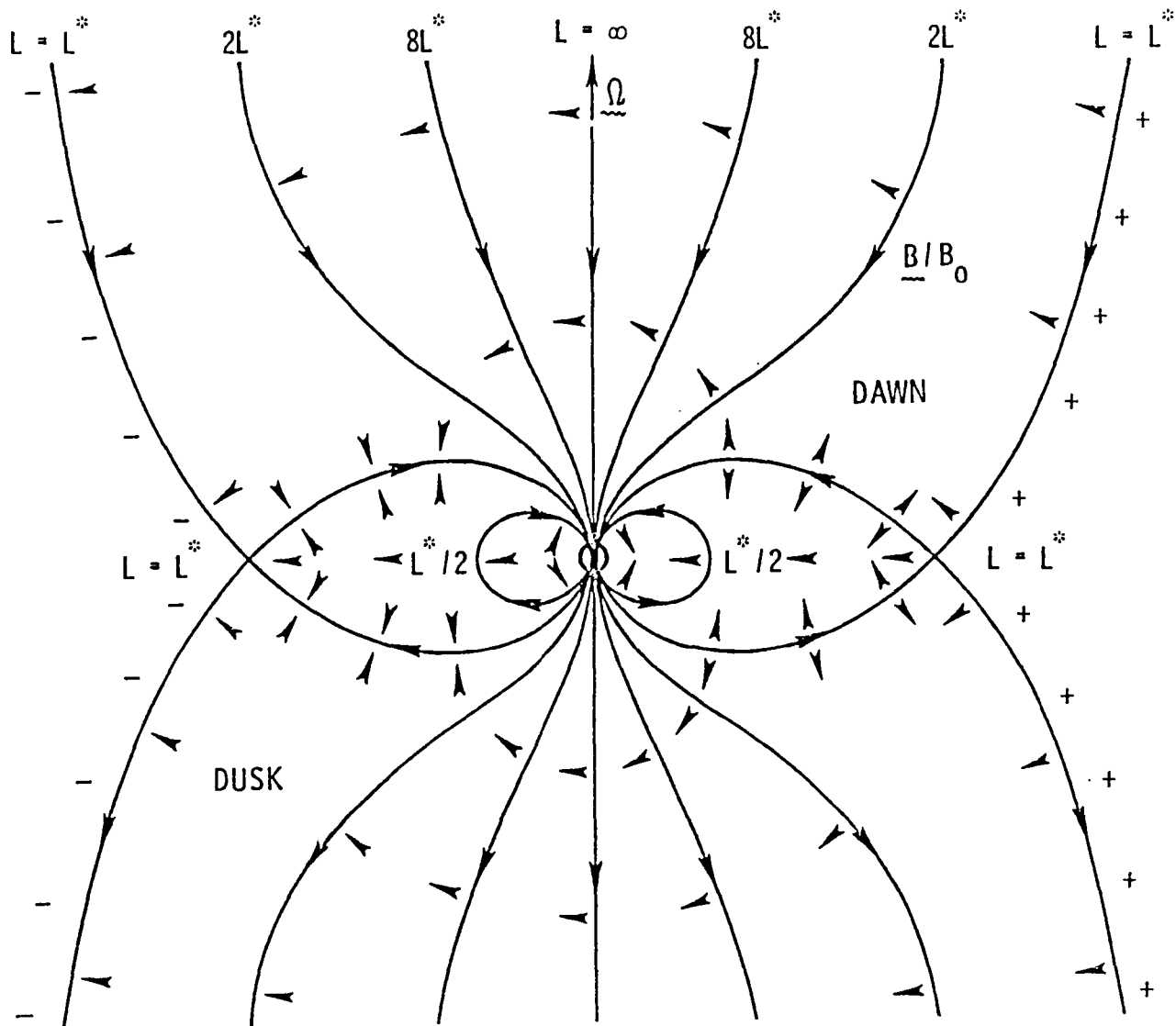


Fig. 1. A schematic illustration of magnetospheric structure showing solid closed and open field lines and their separatrixes L^* . The directions of the magnetospheric electric field are shown by arrowheads attached to field lines. Divergence and convergence of electric fields occur on L^* .

trostatic field without the concomitant appearance of an electric-field component parallel to \vec{B} . This inability is a consequence of current conservation, Pedersen conductivity, and ohmic resistivity in the ionosphere [Chiu, 1974]. Moreover, the hot collisionless magnetospheric plasma in the same flux tube supports such a parallel (to \vec{B}) electric field and thus causes the E_{\parallel} to remain substantial, even at altitudes up to about 10^4 km. The signature of this E_{\parallel} (upward in the PM sector) is plainly evident in ion and electron distributions observed from the S3-3 satellite [Mizera and Fennell, 1977]. The indicated E_{\parallel} signature at the boundary layer in the evening sector is also confirmed [Mozer et al., 1980].

On the morningside, these conditions favorable to discrete arc formation by magnetosphere-ionosphere coupling are not met. Indeed, if an E_{\parallel} can be supported in the morning sector in this admittedly simple scheme, it would be downward and thus accelerate electrons upward. Yet, auroral arcs due to electron precipitation are plainly evident in the morning sector; thus, a global kinetic theory of magnetosphere-ionosphere coupling remains incomplete unless a theory of morningside auroral arc formation consistent with the evening sector is formulated.

We have constructed a theory of morningside auroras based on modulation of the diffuse auroral electron precipitation into bands or striations of characteristic perpendicular scale, which is typically of the order of several auroral ion gyroradii. Modulation of the diffuse auroral electron precipitation is presumed to result from modulation of the wave intensities responsible for scattering the auroral particles into the loss cone. This can happen, for example, if an ULF instability modulates the plasma density and/or magnetic-field strength near the magnetospheric equator and thereby modulates the growth rate for some VLF wave mode, either electromagnetic [Coroniti and

Kennel, 1970] or electrostatic. The result could be a pulsating aurora. Such modulation could also occur near zero frequency and be nonconvective if the background plasma density is nearly uniform, as in the diamagnetic mirror instability [e.g., Scarf et al., 1967]. In this case, the auroral modulation need not be associated with micropulsations. Hasegawa [1969] has, of course, pointed out that the mirror instability becomes convective when the magnetic field is inhomogeneous, and it seems clear that a perpendicular electric field would also make the instability convective. However, the least convective excitations of the mirror instability would seem to be those for which the propagation vector is most nearly perpendicular to the drift velocity of the hot plasma, i.e., of the plasma that is making the mirror mode unstable. The result should be a family of striations, roughly parallel to the discrete-auroral oval, but in the diffuse aurora. These striations would be passed on in the usual way from (a) striations in the equatorial B-field intensity and hot-plasma density, to (b) striations in the growth rates of electron-cyclotron waves (either electromagnetic or electrostatic), to (c) striations in the wave intensities, to (d) striations in the electron-precipitation rate and (perhaps more importantly) in the resonant-electron energy required for precipitation, and to (e) striations in the optical characteristics of the diffuse aurora. Such a mechanism might account for the appearance of multiple "arcs" and patches in the diffuse aurora of the post-midnight sector. The supply of electrons for precipitation would not necessarily be depleted by this process, since the drift shells of hot electrons and hot protons intersect obliquely with each other and with the drift shells of cold plasma, along which the striations would tend to be aligned approximately.

In Section II of this report, we shall first review the plasma and optical observational evidences on the morningside aurora. In Section III we shall

discuss the properties of magnetospheric plasma distributions as they are acted upon by the convection electric field. We demonstrate, with interpretive support from subauroral plasma observations of the SCATHA satellite, that auroral ion distributions driven anisotropic by the convection electric field are favorable to driving the mirror instability in the morning sector, which is discussed in Section IV. In Section V, we offer plausible conditions under which a selection of the mirror instability wave number vector (\vec{k}) can develop in the presence of shear in the convection flow. If verified, this conjecture would clarify the relationship between multiple auroral bands and auroral patches — both dominant features on the morningside. In Section VI, we complete the theory by presenting the result of a phenomenological model of the spatial modulation of auroral electron precipitation by the mirror instability.

This theory of the morningside aurora, when merged with the kinetic theory of evening discrete arcs, may be construed as steps towards a global kinetic theory of auroral arc formation.

II. MORNINGSIDE AURORAS

When observed on a coarse scale, the auroral oval seems to be occupied by a single continuous belt of auroral luminosity. However, when observed with finer resolution, the optical morphology of auroral arcs shows very distinct differences between the evening and morning sectors [see, for example, Akasofu, 1976, 1981; Akasofu and Kan, 1981; Oguti, 1981]. Figure 2 shows a schematic diagram [Akasofu and Kan, 1981] which distills the main optical characteristics of the auroral morphology in various local time sectors.

In the morning sector, Fig. 2 shows a multiple system of thin, diffuse and convoluted arcs in which the marked distinction between the discrete and the diffuse auroras is not readily apparent. Indeed, it appears that the diffuse aurora on the morningside is modulated into striations and patches [Akasofu, 1974]. A significant optical characteristic of the morningside aurora is that these features are frequently associated with pulsation [Oguti, 1981; Royrvik and Davis, 1977; Johnstone, 1978]. Further, it has been known for a long time that morningside pulsating auroras have an electron spectrum showing a high-energy tail (> 10 keV) rather than a mono-energetic beam (< 10 keV). This difference is illustrated in Fig. 3. Moreover, it has been observed [Oguti, 1976; Johnstone, 1978] that pulsating auroral patches drift mostly along electric equipotentials. Thus, the pulsating auroral structure is defined by the warm plasma (< 10 keV), which drifts along electric equipotentials, and is not defined by the drift of the precipitating hot electrons (> 10 keV), which excite the optical signature. For the hot electrons, azimuthal gradient drift effects can be more dominant; thus their drift trajectories can depart drastically from convection equipotentials. The significant implication of this feature of morningside auroras is that (a) the forma-

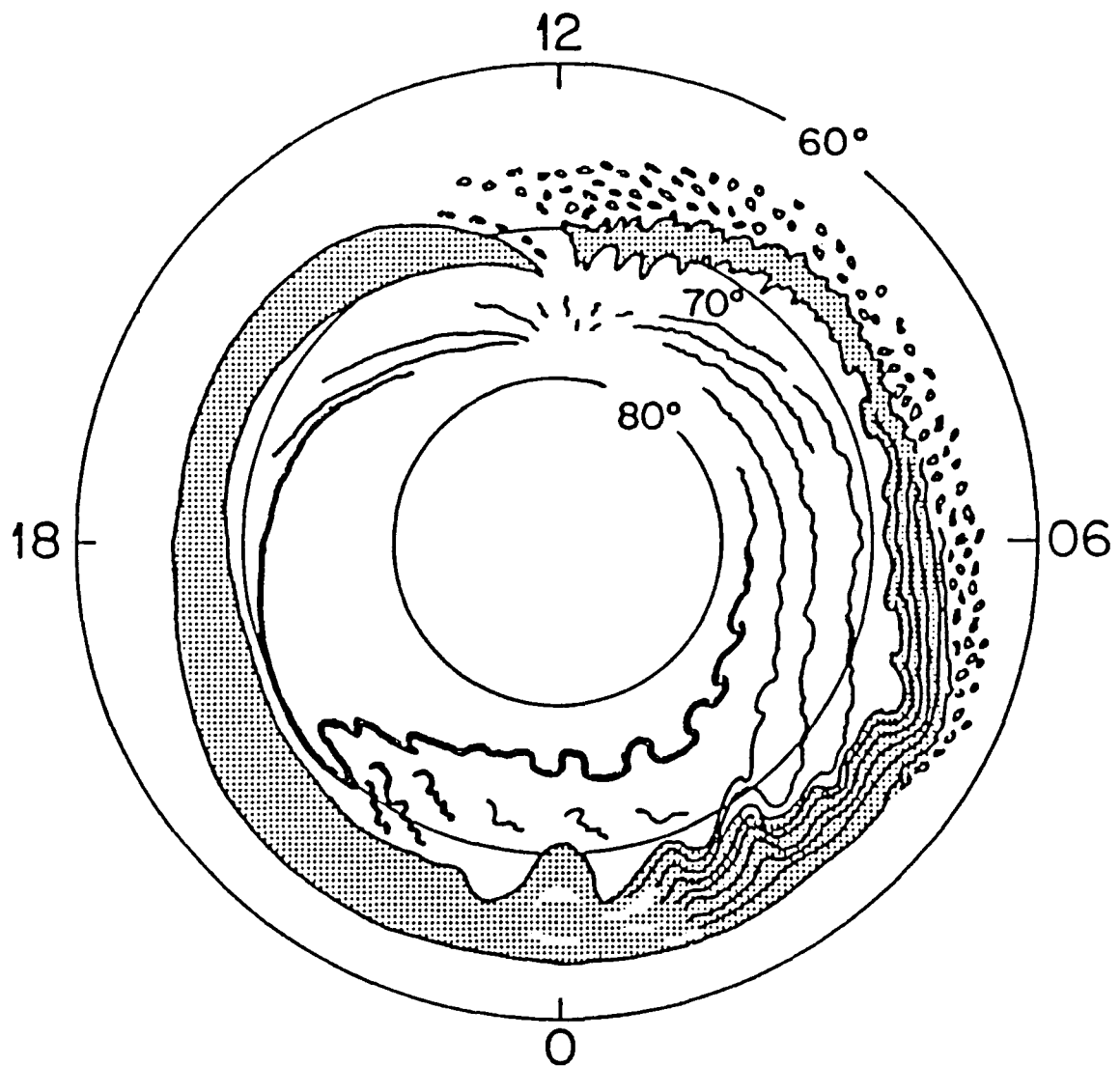


Fig. 2. Auroral morphology (Courtesy of Akasofu and Kan, 1981). Features of interest to this report are multiple striations and patches of the morningside. High-latitude arc systems are to be distinguished from these.

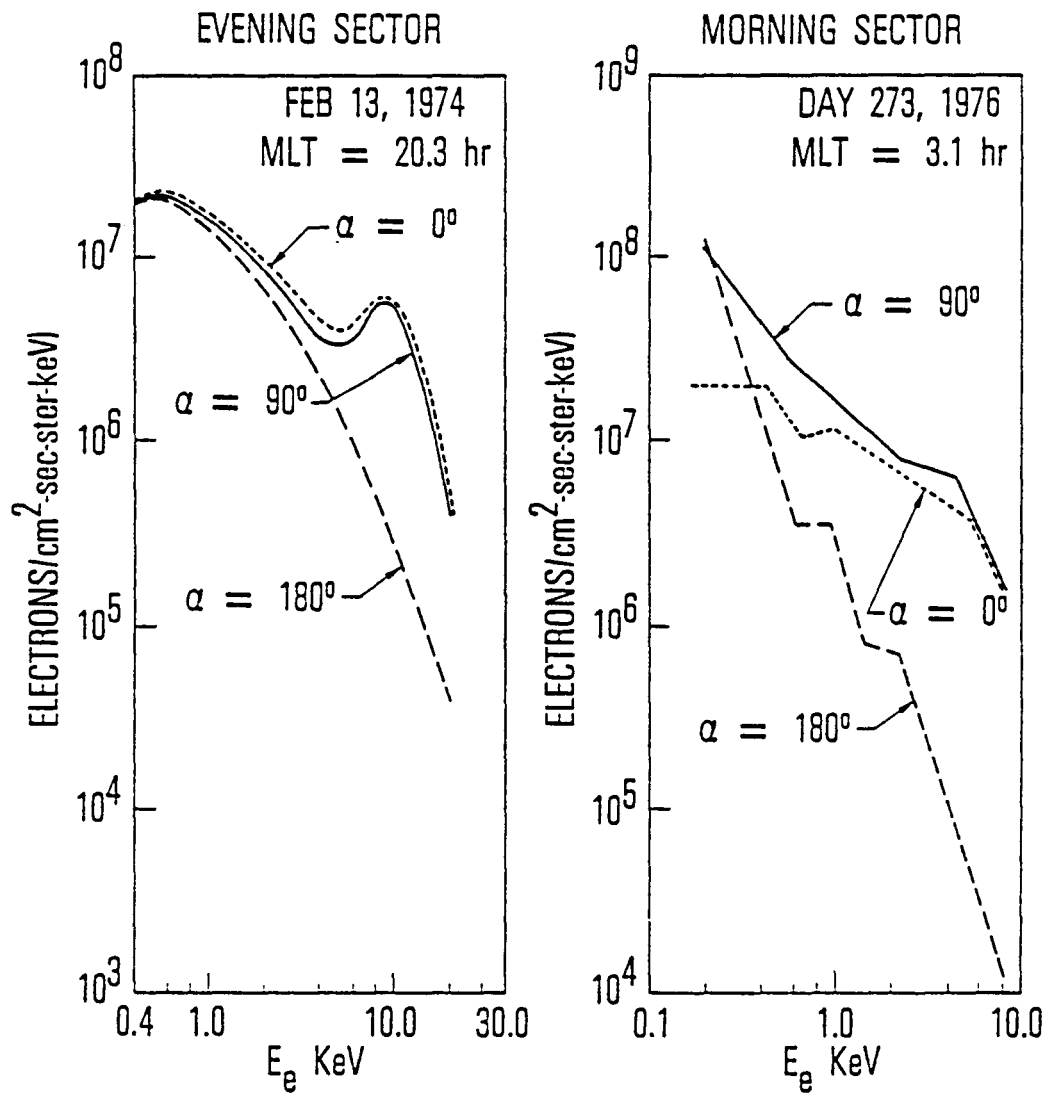


Fig. 3. Typical electron energy spectra measured by the S3-3 satellite in the evening and morning sectors. Spectra at various pitch angles (α) are shown.

tion mechanism of the striations and patches of auroral luminosity must be sought in irregularities of the warm (< 10 keV) plasma, and (b) the irregularities of the warm (< 10 keV) plasma must be able to modulate the precipitation of hotter electrons which precipitate and produce the auroral luminosity. We shall see in the following that our theory is consistent with these two observational implications.

Although morphological features cannot be discerned from satellite plasma observations, satellite plasma data on the morningside are a powerful indicator of the kinetic state of the plasma forming the aurora. Unfortunately, due to the predominant research interest in evening inverted-V structures, very little auroral plasma data interpretation for the morningside has taken place. Figure 3a shows a typical evening auroral electron spectrum measured by the S3-3 satellite. In contrast to the electron beam features characterizing the evening discrete arcs of Fig. 3a, the morningside electron spectrum, shown in Fig. 3b, consists of a hardening at ring current energies and no mono-energetic beam. This is entirely consistent with modulation of hot electron precipitation as the cause of multiple morningside arcs. Although no formal statistical measure of the local time preference of these two types of electron spectra has been obtained, the predominant preference of inverted-V precipitation events for the evening sector is well-established. For example, this tendency is plainly evident in the AE-D data [Hoffman and Lin, 1981]. Further, a statistical survey of upgoing ion beams, another element of plasma signature of inverted-V structures, has been made [Gorney et al., 1981] and the results show definite preference for ion beams to occur in the evening sector while few ion beams are found in the morning sector. A particularly succinct summary of the differences between auroral plasma characteristics at $\sim 1 R_E$ altitude is shown in Fig. 4. In this symmetrical pass of the S3-3

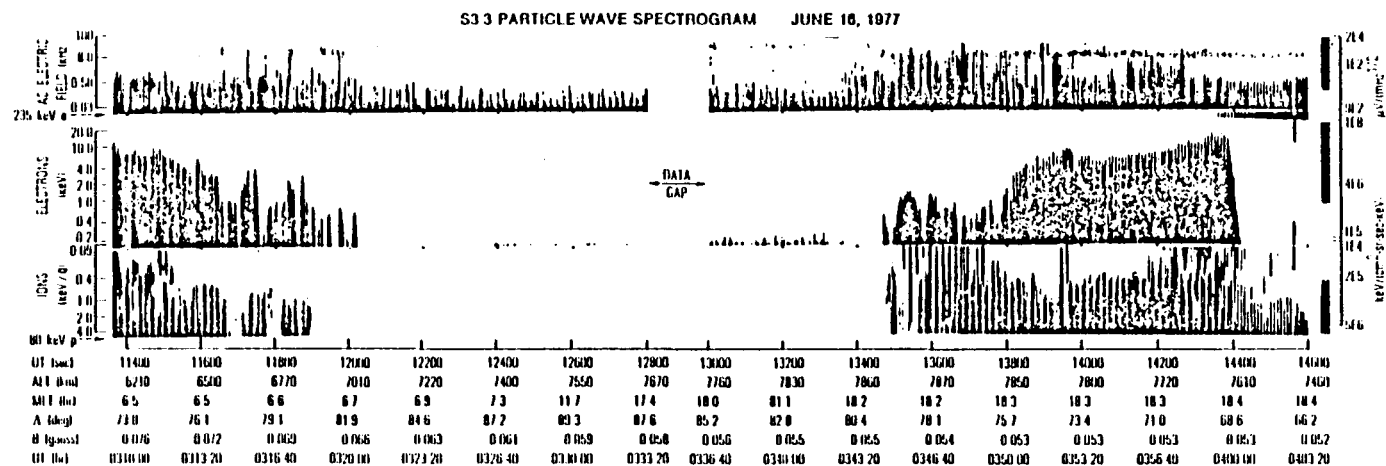


Fig. 4. Energy-time spectra of a dawn-dusk pass of the S3-3 satellite. The top panel is a wave frequency vs. time plot of the pass.

satellite across the auroral oval, it is seen that the simultaneous occurrence of an electron inverted-V and an ion beam indicates parallel potential drops in the evening sector both above and below the satellite, while, on the morningside, the absence of both features in the plasma observations is evidence that the morningside aurora is not associated with electric potential structures, either above or below the satellite. (For a detailed interpretation of features such as in Fig. 4, see Chiu et al., 1982.)

At whatever local time, the plasma distributions at the equatorial regions of auroral field lines are crucial to any aurora formation theory. Unfortunately, direct measurements of equatorial auroral plasmas are not available on a continuous basis. However, invoking the concept of plasma convection in the magnetosphere, features of equatorial auroral plasmas can be reconstructed from equatorial subauroral and near-auroral observations such as those of the SCATHA satellite [Fennell et al., 1981]. Since these data are crucial to the construction of our theory, we need to devote special attention to them; therefore, we defer discussion to the next section where convection of plasma distributions in the magnetosphere is treated.

Meanwhile, we note the following observational features which distinguish morningside from eveningside auroras:

1. Multiple thin arc systems and patches dominate in the morning, and single discrete arc in the evening.
2. Inverted-V electron precipitation structures and ion beams are primarily evening features, indicating absence of parallel electric acceleration in the morning.
3. Morningside electron spectra, similar to the typical diffuse aurora, generally show power-law type hardening at energies higher than a few keV. These spectra are distinctly different in that the mono-energetic downward

electron beam is missing.

4. Morningside optical features are seen to drift with the warm (< 10 keV) plasma, not with the energetic electrons which produce the optical features themselves.

5. Pulsating patches, a predominantly morningside phenomenon, exhibit characteristics consistent with items 3 and 4 above.

6. Quasi-periodic recurrent auroral patches exist in the dawn sector.

III. FORMATION OF PLASMA DISTRIBUTIONS

To construct a global theory of auroral arc formation, one must incorporate the plasma and field features dictated by global boundary conditions, which in turn provide information about how and from where the hot auroral plasmas originate. Virtually all current ideas on the supply and maintenance of hot auroral plasmas invoke inward convection of plasmashet particles. In the simplest form, the inward convection hypothesis assumes that a single uniform population of isotropic ions ($T_i \sim 2 - 3$ keV) and electrons ($T_e \sim \frac{1}{2} - 1$ keV), found well inside the plasmashet [Frank et al., 1981], is convected adiabatically inward past the auroral zone and perhaps deep into the plasmasphere. This simple theoretical concept is appealing in many respects, but it requires testing by comparison with plasma observations in (or near) the equatorial regions of auroral and/or sub-auroral field lines. We shall see in this section that plasma observations of the SCATHA satellite imply essential modifications of this simple concept. These modifications of the inward convection hypothesis of hot plasmas, taking into account hot ions of ionospheric origin, are a key element in constructing our theory of morningside multiple auroral bands, although the most important element of time-dependence [Chiu and Kishi, 1983] will be dealt with elsewhere.

When the SCATHA satellite was recognized to be near the equatorial regions of auroral (and/or near auroral) field lines, the plasma instruments onboard measured typically two types of ion distribution functions and a typical electron distribution function with anisotropy perpendicular to the magnetic field (\vec{B}). The two types of ion distribution functions are shown in Figs. 5a and 5b, and the typical electron distribution function is shown in Fig. 6. In both ion and electron distributions, it is seen that the more

IONS 11 FEB 1979

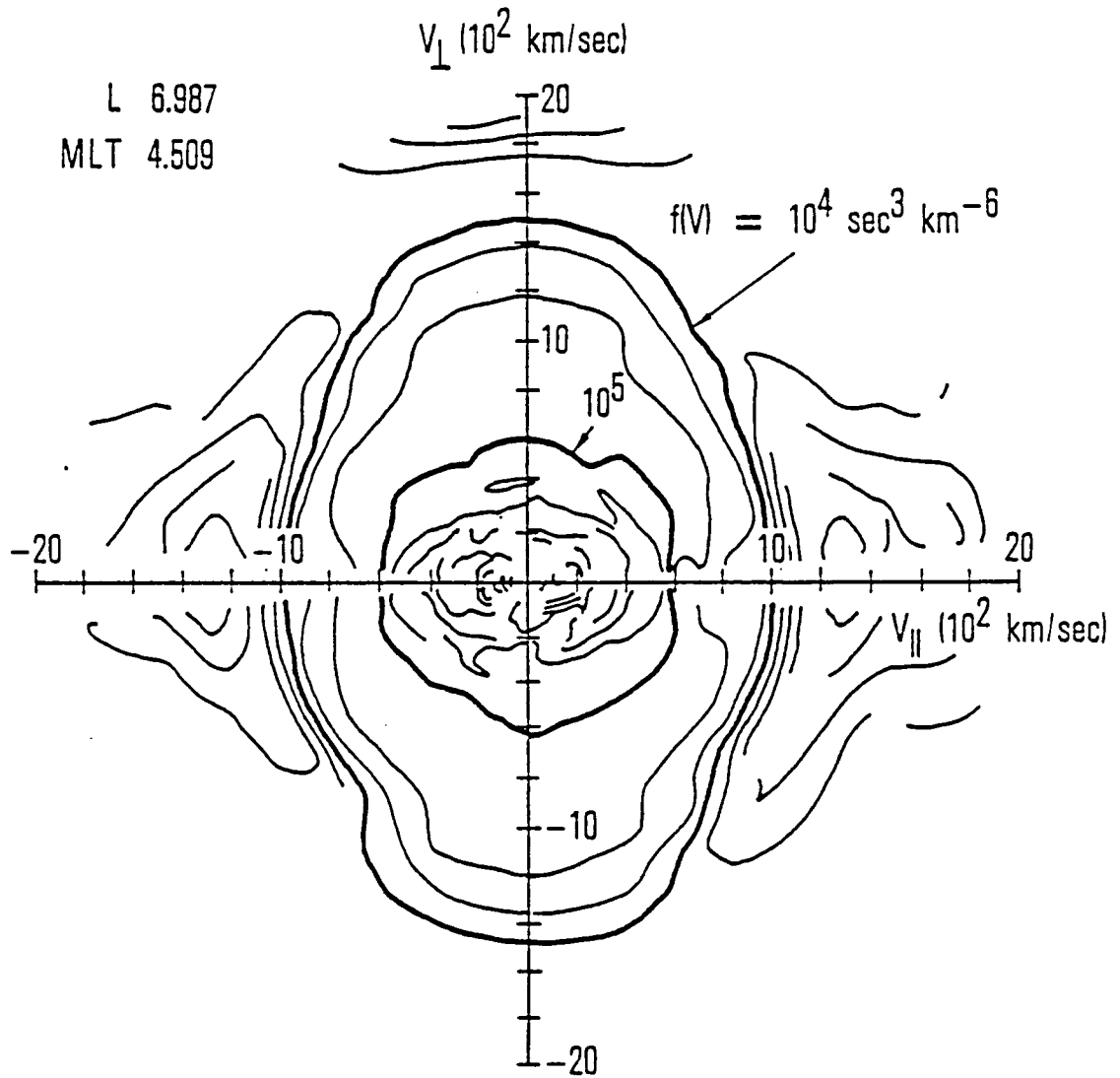


Fig. 5a. Typical dominantly field-perpendicular ion distribution measured by the SCATHA satellite.

IONS 15 NOV 1979

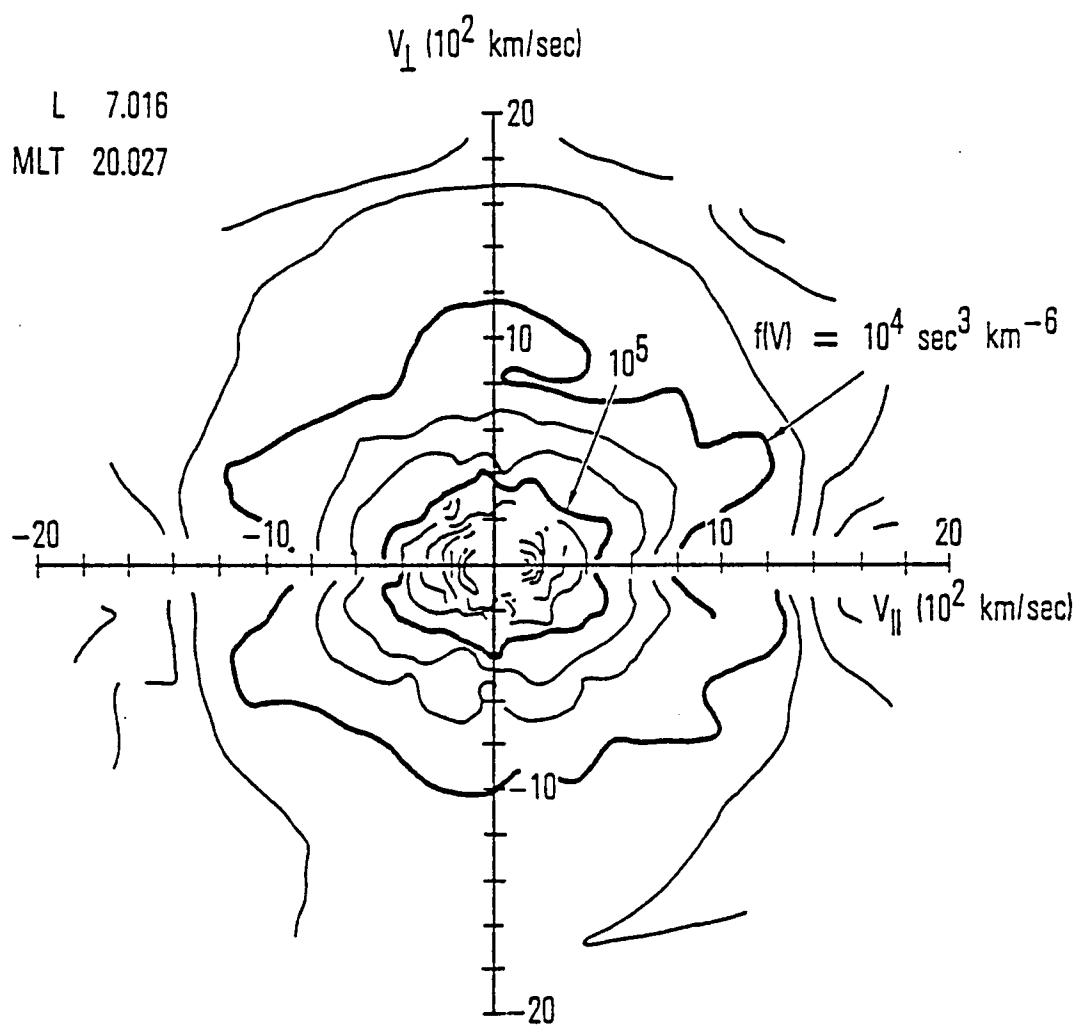


Fig. 5b. Typical dominantly field-aligned ion distribution measured by the SCATHA satellite.

ELECTRONS 15 NOV 1979

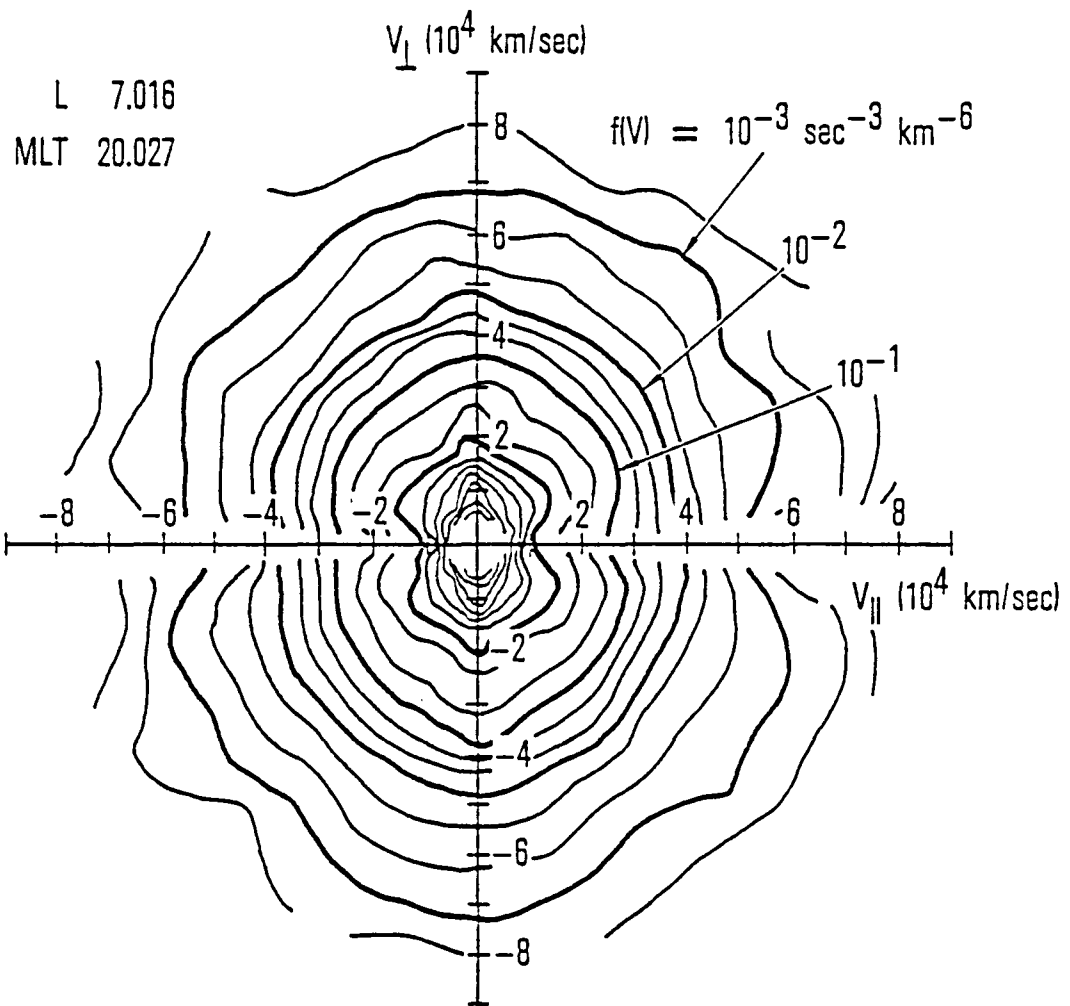


Fig. 6. Typical electron distribution measured by the SCATHA satellite.

energetic populations are anisotropic in the v_{\perp} -direction, as one would expect if these particles were convected in from the plasmasheet. For the ions, a low-energy component, anisotropic in the v_{\parallel} -direction, is almost always present but in varying strength (see below). The presence of O^+ in this field-aligned component indicates strongly that it originates from the discrete aurora [Fennell et al., 1981; Kaye et al., 1981]. The field-alignment and composition strongly suggest that these ions are the low-energy remnants of ion beams accelerated upward by the electric potential structure associated with the auroral discrete arc. Since the discrete arc and inverted-V structures are primarily evening and midnight phenomena, the relative dominance of these low-energy field-aligned ions should also reveal a preference for the evening and midnight sectors. Fennell et al., [1981] distinguished the field-aligned dominant distribution of Fig. 5a from the field-perpendicular dominant distribution of Fig. 5b by the value of the energy corresponding to the separatrix between the field-perpendicular and field-aligned distribution function contours (the transition energy). Thus, the transition energy of Fig. 5a is greater than that of Fig. 5b. Fennell et al., [1981] showed a plot of this transition energy as a function of magnetic local time for almost three days of SCATHA data [Fig. 7]. Although real-time geomagnetic activity obviously plays a role in the increase of the field-aligned population, we note that increases generally take place in the 18-03 MLT sector where the discrete arcs are generally located. Further, as one approaches the morning sector (after 04 MLT), the field-aligned population shows a fading trend. Thus, at the morning sector, on near-auroral field lines, the dominant energetic ion population is that of plasmasheet origin, as indicated by the perpendicular pitch angle anisotropy of Fig. 5a. Although the demarcations between "evening-like" and "morning-like" trends in Fig. 7 are not sharp and vary from day to day, we

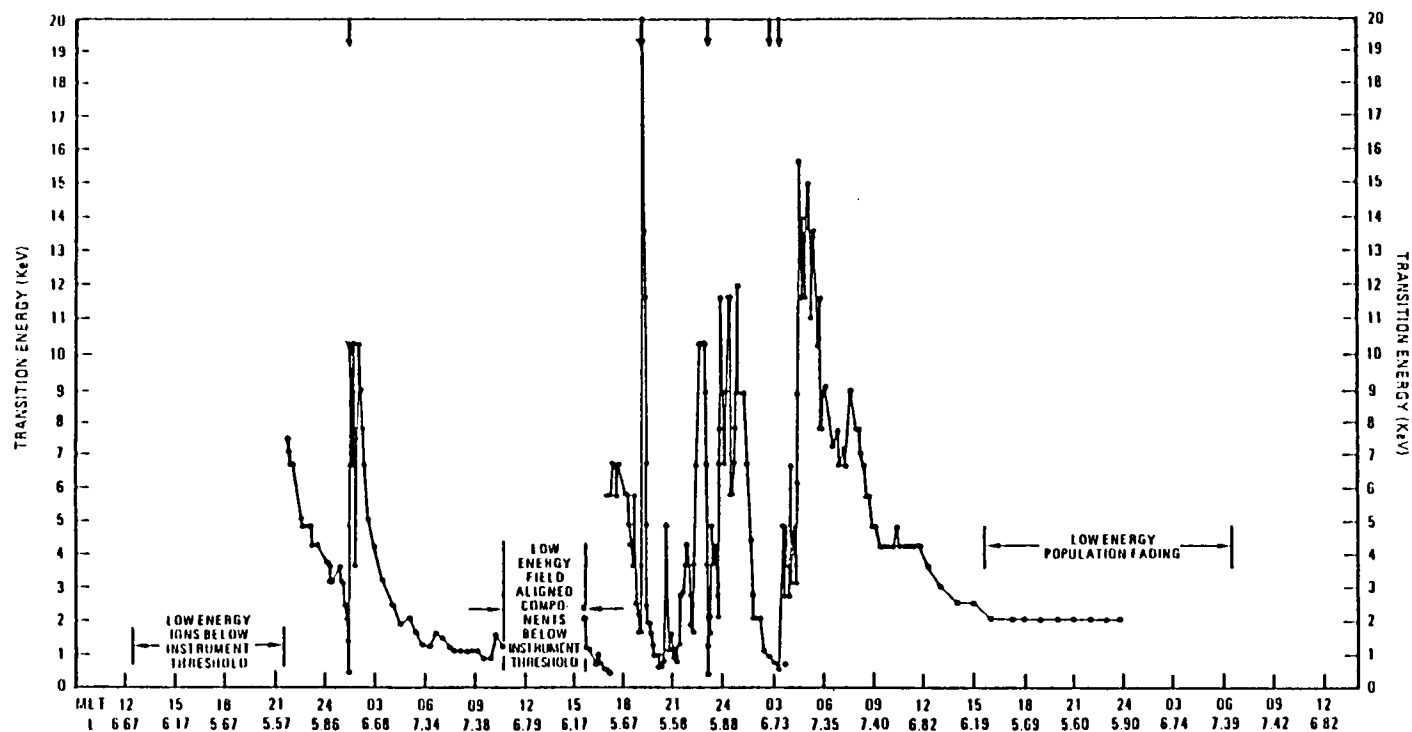


Fig. 7. Local-time dependence of the transition energy between field-aligned and field-perpendicular populations such as shown on Figs. 5a and 5b.

stress that these trends are consistent with the preferred locations of ion beams and inverted-V's, and with the inward convection hypothesis. In this report we shall assume the above interpretation and examine its consequences.

We shall argue in the next section that the field-perpendicular populations of ions favor generation of mirror instability at or near zero-frequency in the morningside auroral zone, whereas the presence of the lower-energy (< 10 keV) field-aligned population in the late evening sector suppresses mirror instability in the auroral region, thus accounting for an important difference between evening and morning auroras.

From the above description and qualitative interpretation of the distribution functions and transition energies of Figs. 5-7, it is rather obvious that the appearance of hot plasmas in auroral and sub-auroral equatorial regions can no longer be considered in terms of time-independent convection of a single component of plasma from the plasmashet. In short, the causal implications of injection in real time, the local-time dependence of the injection source, and, last but not least, the existence of an ionospheric source from the discrete aurora are essential and unavoidable complications that are part and parcel of the inward convection hypothesis for the formation of hot auroral plasmas [Chiu and Kishi, 1983]. Thus, in order to verify theoretically the interpretation of data discussed above, we need to construct nothing less than a causal theory of plasma injection and convection in the equatorial magnetosphere, taking into account spatial and temporal factors of both the sources and the convection of plasma distributions. A Green's function solution of such a new time-dependent theory has been formulated and will be dealt with elsewhere [Chiu and Kishi, 1983]. For our purposes here of interpreting Figs. 5a and 5b for the construction of auroral ion and electron distributions, it is sufficient to abstract the local-time (spatial) trend of

Fig. 7 and to focus upon the spatial source distribution underlying Fig. 7, rather than to focus upon the time-dependence of the injection process which complicates Fig. 7 in the midnight hours. Under this simplification, morning-side and eveningside ion distributions can be considered in terms of a time-independent plasma convection model, which is the present "state of the art" [e.g. Wolf, 1970; Chen, 1970; Kivelson et al., 1979; Kivelson and Southwood, 1975; Cowley and Ashour-Abdalla, 1975; Kaye et al., 1979].

In such a static model, plasma is driven by the convection-corotation electrostatic potential [Volland, 1975]

$$\phi(L, \phi) = \phi_c L^{n+1} \sin\phi + \phi_r/L \quad (1)$$

where $n=1$ is an assumed parameter, ϕ_c is a measure of the cross-tail potential drop, and $\phi_r = -91$ kV is a measure of the dipolar corotation potential. Figure 8 shows an equipotential contour plot of (1), with $\phi_c = -0.43$ kV (roughly appropriate for storm time). For the plasmasheet source distribution, we assume a uniform nightside (dawn to dusk) Maxwellian distribution of ions and electrons at $L=13$. In the evening sector, we assume field-aligned ion beams are to be injected at $L=10$ by both the northern and southern discrete arcs, since distinct counter-streaming ion beams are often seen even at SCATHA latitudes. The ion beams are assumed to have drift energies of < 10 keV and Maxwellian temperatures of similar magnitude. Plasma distributions from these two sources are assumed to be adiabatically convected to the location of SCATHA at $L \sim 7$ at various local times. The source distribution function is given below:

$$f = N_M \left[\frac{m_M}{2\pi T_M} \right]^{3/2} \cdot \exp\left[-\frac{m_M v^2}{2T_M}\right] \cdot g(L, \phi)$$

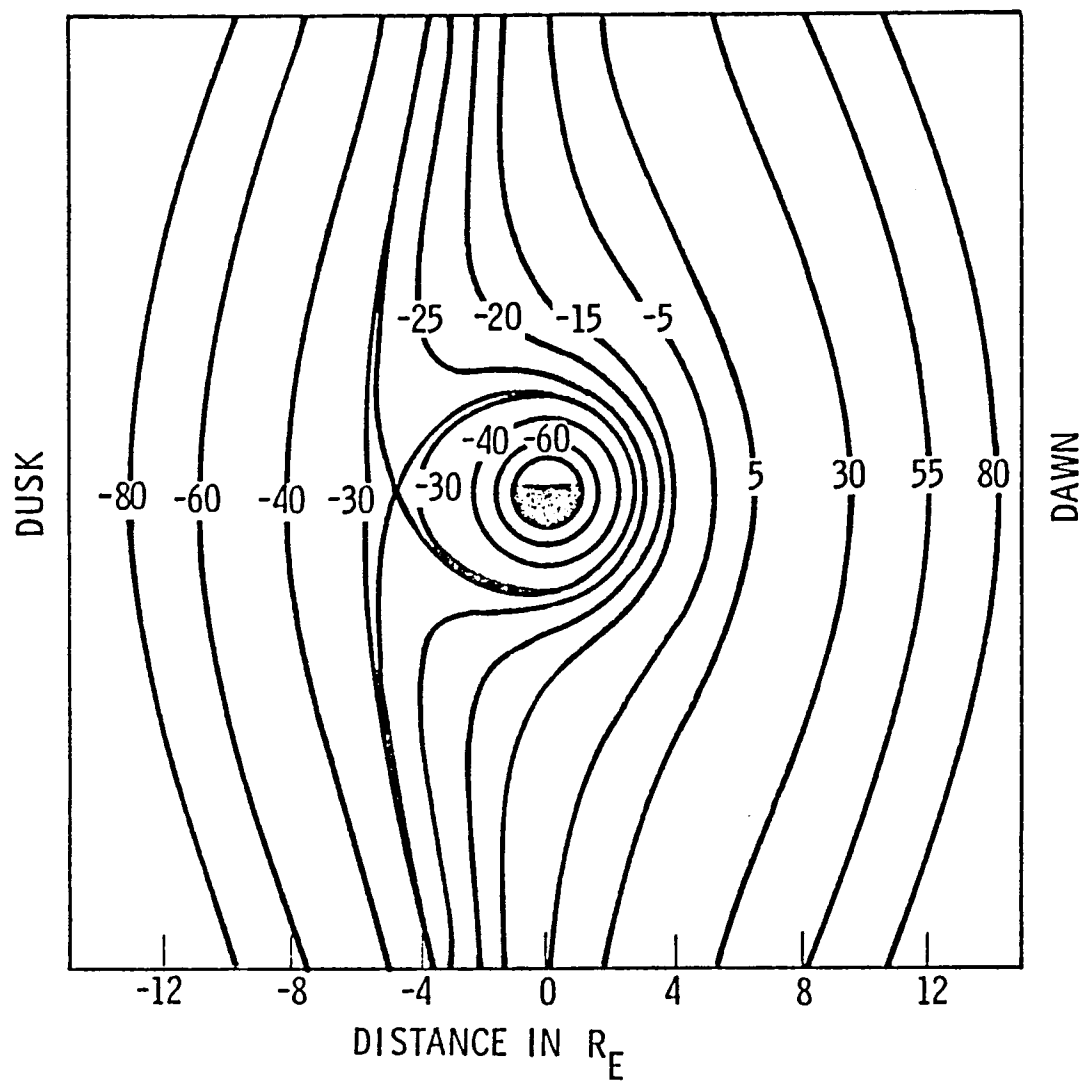


Fig. 8. Equipotential contours (in kV) of a simple convection electric field model according to Eq. (1) (Volland, 1975).

(2)

$$+ \sum_{v_A = \pm} N_A [m_A / 2\pi T_A]^{3/2} \cdot \exp[-m_A (v - v_A)^2 / 2T_A] \cdot h(L, \phi)$$

where the subscripts M and A denote plasmasheet and discrete auroral sources, respectively. The spatial functions g and h are as described above:

$$g = \delta(L - L_M) \theta(\phi - \pi/2) \theta(3\pi/2 - \phi) \quad (3)$$

$$h = \delta(L - L_A) \theta(\phi - \pi/2) \theta(\pi - \phi) \quad (4)$$

where ϕ is measured clockwise from noon MLT ($\phi = 0$).

The adiabatic mapping of a particle of mass m and charge qe from the phase space point $(\vec{v}_0, \vec{r}_0) \equiv (v_0, \alpha_0, L_0, \phi_0)$ to the phase space point $(\vec{v}, \vec{r}) \equiv (v, a, L, \phi)$ requires conservation of the magnetic moment

$$v L^{3/2} \sin \alpha = v_0 L_0^{3/2} \sin \alpha_0 \quad (5)$$

and conservation of energy

$$W_0 \equiv \frac{1}{2} m v_0^2 + qe\phi(L_0, \phi_0) = \frac{1}{2} m v^2 + qe\phi(L, \phi) \equiv W \quad (6)$$

In addition, the conservation of the bounce invariant is assumed to be given by the approximate relation [Southwood and Kivelson, 1975]

$$\frac{\sin \alpha}{\sin \alpha_0} = [\sin \alpha_0 + (L/L_0)^{0.45} (1 - \sin \alpha_0)]^{-1} \quad (7)$$

Figures 9a and 9b show an example of our source model distribution mapped to two observation points: (a) $L = 7$, $\phi = \pi/2$ and (b) $L = 7$, $\phi = 3\pi/2$. We have assumed $T_M = 1$ keV and $T_A = 1/2 m_A v_A^2 = 0.5$ keV. These model parameters, together with the relative values of N_M and N_A , can be chosen to fit the important population components of Fig. 5a. The upper energy cutoffs in Figs. 5a and 9a are the effects of Alfvén boundary formation at the L-value of observation. The field-alignment of the lower-energy population in Fig. 9a is due to the merging of two counter-streaming beams of the model, (4). Although Fig. 5a does not show counter-streaming beams at low energies, the counter-streaming ion beam phenomenon is frequently observed in SCATHA data [Richardson et al., 1981]. Since the signature of counter-streaming ion beams is not always present but field-aligned anisotropy is always present in the low-energy component, the auroral source in (4), consistent with Figs. 5a and 5b, can also be modeled as a bi-Maxwellian with field-aligned anisotropy. Indeed, it seems reasonable that the two-stream instability could cause two counter-streaming beams to merge into a field-aligned population [Schulz and Koons, 1972]. This simpler bi-Maxwellian source model, with proper convection-induced cutoffs, is used in illustrating mirror instability calculations, although both counter-streaming and bi-Maxwellian source models can be used with similar effect.

To conclude this section, we note that the systematic local-time related features of SCATHA plasma populations observed at $L \sim 7$ can be understood in terms of relatively simple sources at higher L-values together with the simple concept of inward adiabatic convection. This exercise gives us confidence in the model for L-values between $L = 7$ and the sources.

We shall demonstrate in the next section that morningside field-perpendicular ion distributions such as Fig. 9b can drive mirror instability

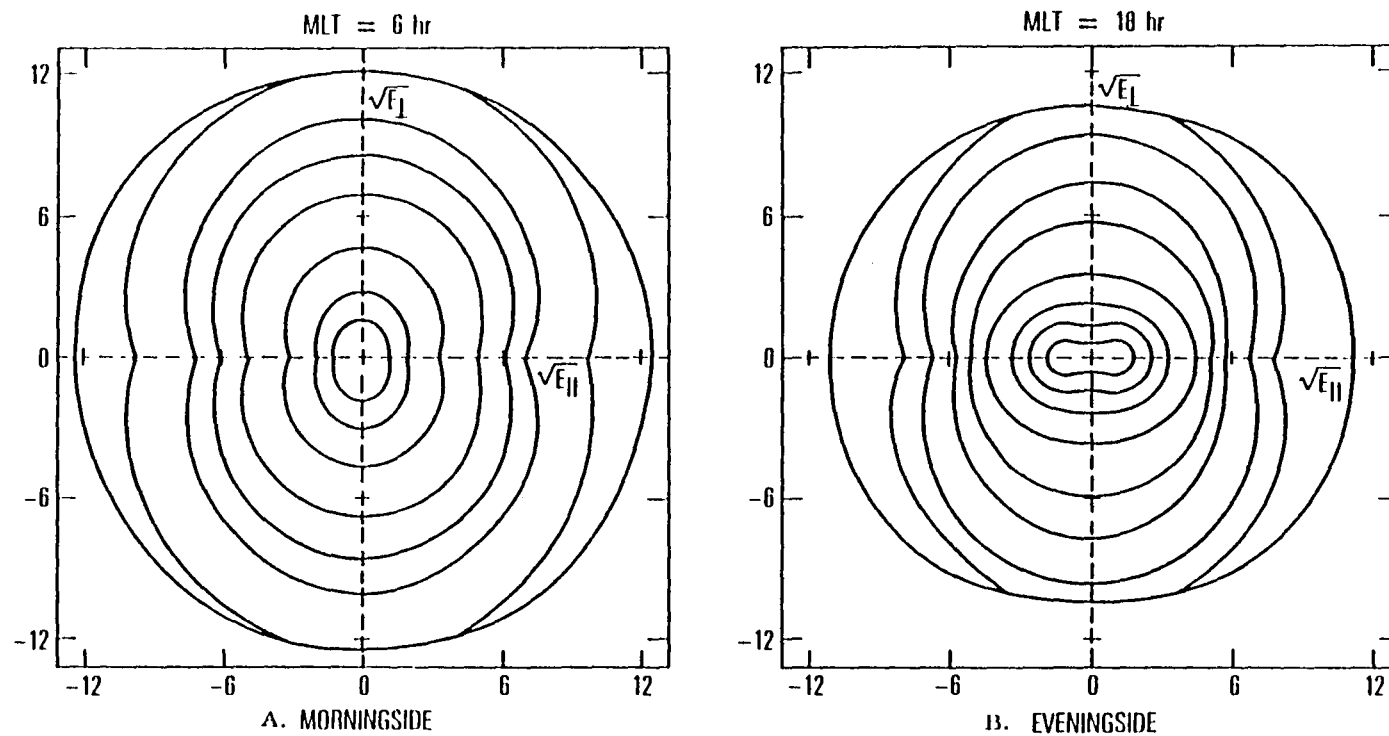


Fig. 9. Simple Maxwellian ion distributions mapped from $L = 13$ to (a) $L = 7$ and dawn, and (b) $L = 7$ and dusk. Field-aligned ion beams are assumed to be injected at $L = 10$ in the evening hours.

at $L = 7-9$, whereas the field-aligned component in the evening, such as in Fig. 9a, can stabilize the effect of the field-perpendicular component so as to inhibit mirror instability in the evening hours, if the auroral source can provide sufficient field-aligned ions of sufficiently high energy.

IV. MIRROR INSTABILITY AND PLASMA CONVECTION

It is known for a long time that a high- β ($\beta \sim 1$) plasma with pressure anisotropy ($\beta_{\perp} > \beta_{\parallel}$) can be unstable to a longitudinal wave mode which is an offshoot of the MHD waves. This instability was named the "mirror" instability because a loss-cone distribution in a mirroring field would have $\beta_{\perp} > \beta_{\parallel}$. In space plasma physics, the mirror instability has frequently been invoked to account for compressional mode micropulsations [Hasegawa, 1969; Lanzerotti et al., 1969] with periods in the > 100 sec range. Hasegawa [1969] showed that in a plasma density gradient the mirror mode merges with drift waves such that the real part of the frequency is the drift wave frequency. At lower L-values, such as near the plasmapause region, such micropulsations, with non-zero frequency and interpreted in terms of the mirror instability, may indeed be very important. Since we are interested in the mirror instability driven by convected plasmasheet ions in the region poleward of the diffuse auroral boundary (mapped to the equatorial plane) in the morning sector where there are no marked cold plasma gradients, we shall not be involved with the micropulsation aspects of the mirror instability, although particle flux modulation is part and parcel of micropulsations. We emphasize that zero-frequency mirror instability need not be correlated to occurrence of micropulsations. In the absence of the real part of the frequency, the mirror instability becomes striations of the plasma and furrows of the magnetic field in space. In the next sections, we shall demonstrate that these striations of the convecting plasma and magnetic field can affect the rate of diffuse auroral electron precipitation.

To determine whether convecting ions can drive the mirror instability, one must show that the distribution functions modeled in the last section

satisfy a criterion [Hasegawa, 1975, pp. 94-99] under which the growth rate can be positive. In the case of bi-Maxwellian plasma, the instability criterion is

$$1 + \beta_{ii} (1 - T_{ii}/T_{ii}) + \beta_{ie} (1 - T_{ie}/T_{ie}) < 0 \quad (8)$$

where $\beta_i = 8\pi n_i/B_0^2$ for both ions (i) and electrons (e). It can be seen in (8) that $T_i > T_e$ and $\beta_i \sim 1$ are required to satisfy the instability criterion. It is our contention that both conditions are satisfied by plasma-sheet ions and electrons injected onto the auroral region because inward-convecting particles gain perpendicular energy preferentially, and substorm plasma at high L-valued equatorial regions are expected to have higher β . In order to demonstrate instability in our model of convected plasma distributions, (8) cannot be used because the distributions shown in Figs. 9a and 9b are obviously not bi-Maxwellians, even though some sources can be bi-Maxwellian.

In the notation of Hasegawa [1969], in which ϵ_{ij} is the i-j component of the plasma dielectric tensor, the relevant dispersion relation to mirror instability in the low-frequency ($\omega/\Omega_i \ll 1$) and long-wavelength ($kv_i/\Omega_i \ll 1$) regime is

$$k^2 - \frac{\omega^2}{c^2} (\epsilon_{yy} + \epsilon_{yz}^2/\epsilon_{zz}) = 0 \quad (9)$$

In the above, k is the wave number, ω is the wave frequency, Ω_j is the cyclotron frequency of species $j = i, e$, and v_j is the thermal velocity. The third term of (9) in the form $(\omega^2/c^2 k^2)(\epsilon_{yz}^2/\epsilon_{zz})$ is of the order of the electron $\beta_e (< 1)$; therefore, the dispersion relation is assumed to be k^2

$-\omega^2 \varepsilon_{yy}/c^2 = 0$, where in terms of a general distribution function f_j and plasma frequency ω_{pj}

$$\begin{aligned} \varepsilon_{yy} = 1 + \sum_{j=i,e} (\omega_{pj}^2/\Omega_j^2) + \\ \sum_{j=i,e} (\omega_{pj}^2/\omega^2 \Omega_j^2) 2\pi \int_{-\infty}^{\infty} dv_{\parallel} \int_0^{\infty} v_{\perp} dv_{\perp} \left\{ k_{\parallel}^2 \left[v_{\parallel}^2 - \frac{1}{2} v_{\perp}^2 \right] f_j - k_{\perp}^2 v_{\perp}^2 f_j \right. \\ \left. - k_{\perp}^2 \cdot \frac{1}{4} v_{\perp}^2 \frac{(\partial f_j / \partial v_{\parallel})}{v_{\parallel} - \omega/k_{\parallel}} \right\} \end{aligned} \quad (10)$$

From (9) and (10), it is a straightforward matter to show that the instability criterion is

$$1 + \frac{8\pi}{B_0^2} \sum_{j=i,e} 2\pi \int_{-\infty}^{\infty} dv_{\parallel} \int_0^{\infty} v_{\perp} dv_{\perp} \left\{ \frac{1}{2} m_j v_{\perp}^2 f_j + \frac{1}{4} v_{\perp}^4 P \frac{(\partial f_j / \partial v_{\parallel})}{v_{\parallel} - \omega/k_{\parallel}} \right\} < 0 \quad (11)$$

where P indicates the principal value integral. In the low-frequency limit (indeed, $\omega \sim 0$ in our case) the resonance denominator in (11) can be expanded, and (8) is obtained if f_j is bi-Maxwellian.

Since the empirical distributions (Figs. 5a and 5b) and the model distributions (Figs. 9a and 9b) are not bi-Maxwellian, a realistic evaluation of the instability criterion (11) requires numerical techniques. We have applied the convected distributions of source models discussed in the previous section to the instability criterion (11) to show that, if the field-aligned auroral ion beam source is sufficiently strong (in number and in energy), the mirror instability driven by the field-perpendicular plasmashet component can be stabilized in the evening sector, thus confining the effects of the mirror instability to the morning sector during strong injection events such as in Fig. 7. To illustrate this point, the source model (4) is not very convenient because the field-aligned anisotropy of the higher-energy portion of the

convected distribution from the auroral source depends on T_A and v_A in a complicated manner. In contrast, the source model with a bi-Maxwellian auroral source (with temperatures $T_{A\perp}$ and $T_{A\parallel}$) is particularly convenient because the field-aligned anisotropy of the convected auroral component (Fig. 9b) is controlled by the source field-aligned anisotropy $T_{A\parallel}/T_{A\perp}$. Figure 10 illustrates the dependence of the indicator of mirror instability, left hand side of the inequality (11), as function of $T_{A\parallel}/T_{A\perp}$ at the source for a given normalization density ratio between the plasmashet and auroral components of Fig. 9b. Thus, if the discrete aurora is sufficiently strong and the ion beam energy is sufficiently high (i.e., the source ions are strongly field-aligned), the mirror instability can be stabilized by the evening discrete arc. On the other hand, the absence of the discrete auroral source on the morningside enhances the likelihood of mirror instability associated with injection events of Fig. 7. For the calculations of Fig. 10, the magnetospheric source is located at $L_M = 11$ instead of $L_M = 13$. For $L_M = 13$, instability can occur at even higher values of $T_{A\parallel}/T_{A\perp}$ than that of Fig. 10.

This new concept of "feedback" by the discrete aurora upon the effects driven by magnetospheric convection is somewhat interesting in that it breaks away from the perception that the aurora is a passive sink driven by solar wind-magnetosphere interactions.

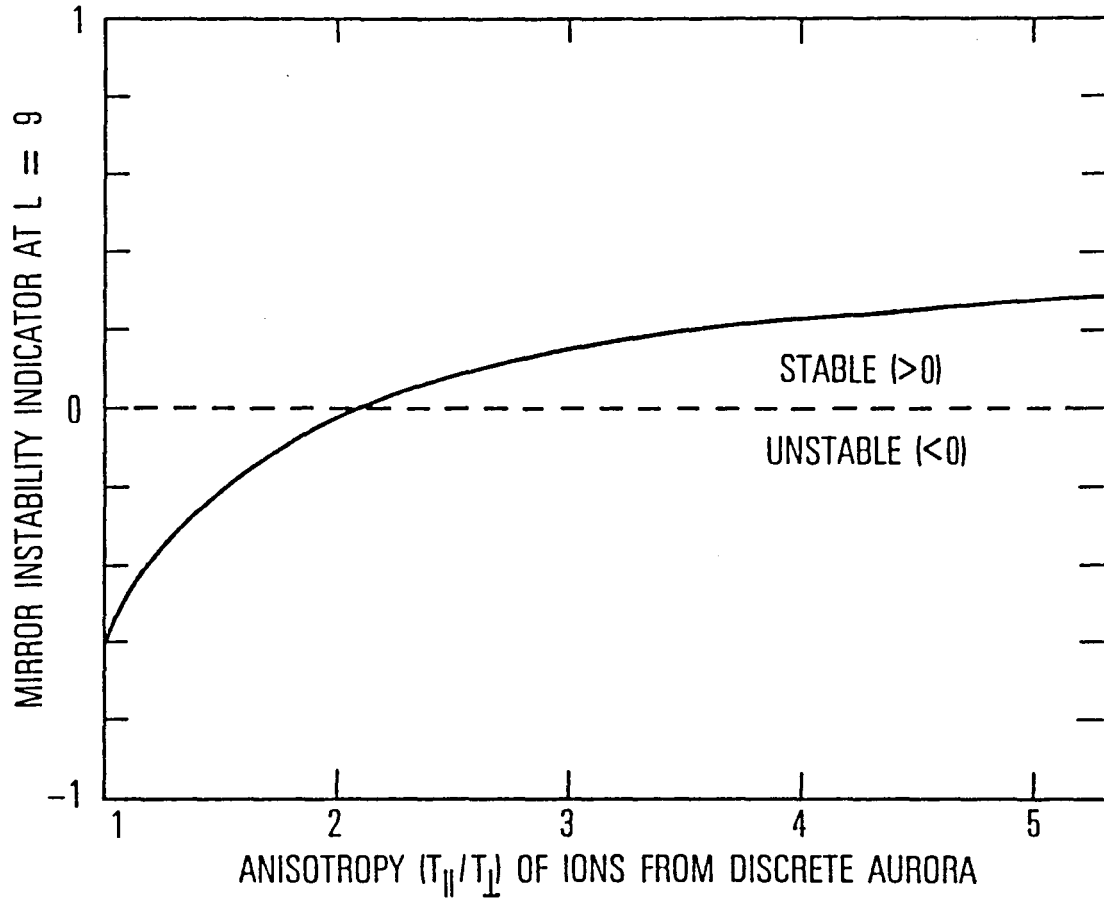


Fig. 10. Dependence of the mirror instability indicator at $L = 9$ [left-hand side of the inequality (11)] on the ion anisotropy T_{\parallel}/T_{\perp} of the discrete aurora.

V. SELECTION OF \vec{k} VECTOR

In order to construct a theory of the multiple bands and patches of the morning sector, it is not sufficient to merely establish instability. A plausible explanation of the scales of the bandedness is necessary. This means examining mechanisms by which a single typical value and direction of the instability wave vector \vec{k} are selected.

For a given \vec{k} the mirror instability manifests itself as a series of growing rarefactions and condensations of magnetic field and plasma occurring in parallel planes. However, the disturbance thus represented by a given \vec{k} does not propagate as if in an elastic medium. Rather, it moves only in association with the drift motion of the underlying plasma. This is the significance of having $\text{Re } \omega = 0$ in (8) - (11), where the mirror instability is analyzed in the drift frame of a uniform plasma.

It follows that in a uniform plasma there is no preferred direction for \vec{k} . In that case the mirror instability should take the form of a jumbled superposition of \vec{k} -vector directions and thus resemble (at least in the plane perpendicular to \vec{B}) the condensation of droplets from a vapor. This morphology may be relevant to the patchiness seen in the equatorward portion of the diffuse aurora in the 04-13 sector of local time (see Figure 2) but cannot describe the azimuthally elongated bands that seem to evolve from the entire diffuse aurora soon after midnight and to persist in the poleward portion of the aurora throughout the AM sector. The presence of such a banded structure suggests the preferential selection of \vec{k} vectors perpendicular to the plasma drift velocity.

A likely selection mechanism involves the presence of velocity shear in the magnetospheric plasma motion. The effect of velocity shear on the mirror instability is to refract the wave-normal vector \vec{k} , with respect to the plasma-velocity vector \vec{u} , so as eventually to align the wavefronts with the streamlines. The refraction process is analogous to the rotation of ranks that would occur down a broad avenue if a phalanx of soldiers were to march in the x-direction with speed u and perpendicular velocity shear du/dy . Let \vec{k} be the rank normal vector. The separation of ranks along the x axis remains constant at $2\pi/k_x$, since the velocity of march is independent of x . The slope of a line normal to the ranks is $\pm k_y/k_x$. The ambiguity of sign stems from the possibility of constructing either a forward (+) or a backward (-) rank normal. It follows that for rectilinear motion the rank-normal direction θ evolves according to

$$\tan \theta(t) \equiv k_y/k_x = \tan \theta(0) \mp (du/dy)t \quad (12)$$

and approaches $\mp \pi/2$ as $t \rightarrow +\infty$, as one would expect.

The ranks of soldiers in this allegory represent plasma condensations or rarefactions associated with the diamagnetic mirror instability, and the marching velocity \vec{u} represents the plasma-drift velocity across the magnetic field \vec{B} . The rank-normal vector \vec{k} represents the wave-normal vector, and the rank-normal angle θ represents the wave-normal angle $\cos^{-1}(\hat{k} \cdot \hat{u})$. The foregoing results already imply that θ approaches $\mp \pi/2$ as $t \rightarrow +\infty$, i.e., that the plasma condensations and rarefactions become aligned with the drift-velocity streamlines. However, in the plasma context it is equally important to note that

$$\begin{aligned}
k_{\perp}(t) &\equiv (k_x^2 + k_y^2)^{1/2} = \{[k_x(0)]^2 + [k_y(t)]^2\}^{1/2} \\
&= \{1 + [\tan \theta(0) + (du/dy)t]^2\}^{1/2} |k_x(0)| \quad (13)
\end{aligned}$$

where $k_{\perp}(t)$ is the magnitude of the vector $\vec{k} \times \hat{B}$. For $k_x \neq 0$ one finds that $k_{\perp}(t)$ will increase without limit as $t \rightarrow +\infty$. Now since the maximum growth occurs for $k_{\perp}\rho_i \sim 1$, where ρ_i is the mean ionic gyroradius [Hasegawa, 1969], modes with $k_x \neq 0$ are not favored for growth. Thus, the presence of shear in the plasma drift-velocity field favors the excitation of mirror-mode striations for which k_y is initially of order ρ_i^{-1} and for which k_x is initially zero. The striations, in other words, are preferentially aligned with streamlines of the velocity field.

The magnetospheric situation is slightly complicated by the fact that "hot magnetospheric plasma" does not have a unique drift velocity at any point in space, since the gradient-curvature component of that drift depends on the energy and pitch angle of the individual particle. A unique drift velocity could be defined, of course, by averaging over the energy spectrum and pitch-angle distribution at each point in space. However, it should be sufficient for the purpose at hand to observe that shear is present in the $\vec{E} \times \vec{B}$ drift associated with magnetospheric convection, and that gradient-curvature drifts are typically much smaller than $\vec{E} \times \vec{B}$ drifts for particles representative of the inner plasmashet. For example, the ratio of gradient-curvature drift to convection velocity at $L \sim 8$ is roughly the ratio of particle energy to 10 MeV.

The magnetospheric situation is further complicated by the fact that $\vec{E} \times \vec{B}$ drifts are not rectilinear, thus a tensor quantity is needed to express the presence of shear in the drift-velocity field. One must analyze the shear

tensor [e.g., Morse and Ingard, 1968, pp. 272-273] specified in rectangular coordinates by the expression

$$S_{ij} = (1/2) [(\partial u_i / \partial x_j) + (\partial u_j / \partial x_i)] - (\delta_{ij} / 3) \nabla \cdot \vec{u} \quad (14)$$

in which $x_1 = x$, $x_2 = y$, and $x_3 = z$. For the field model illustrated in Fig. 7, both \vec{E} and \vec{B} are derivable from scalar potentials. It follows that

$$\begin{aligned} \nabla \cdot \vec{u} &= \nabla \cdot [(c/B^2)(\vec{E} \times \vec{B})] \\ &= (c/B^2) [B \cdot (\nabla \times \vec{E}) - \vec{E} \cdot (\nabla \times \vec{B})] \\ &\quad - 2 (c/B^3)(\vec{E} \times \vec{B}) \cdot \nabla \vec{B} \\ &= - (2/B) \vec{u} \cdot \nabla \vec{B} \end{aligned} \quad (15)$$

after application of well-known vector identities [e.g., Panofsky and Phillips, 1962, p. 471]. The electric field $\vec{E}(= -\nabla\phi)$ is derivable from (1) if the dipolar relationship $L \equiv (r/a) \csc^2 \theta$ is inserted there. The coordinates r and θ denote geocentric distance and colatitude, respectively. The magnetic field is given by

$$\vec{B} = (\mu/a^2) \nabla [(a/r)^2 \cos \theta] \quad (16)$$

where a and μ represent the radius and magnetic moment, respectively, of the earth. Evaluation of $\vec{u} = (c/B^2) \vec{E} \times \vec{B}$ in the equatorial plane leads to the simple expressions

$$u_x = - (c/\mu) [(\phi_c/a^2)(x^2 + y^2)(x^2 + 2y^2) - \phi_r ay] \quad (17a)$$

and

$$u_y = (c/\mu) [(\phi_c/a^2)(x^2 + y^2) xy - \phi_r ax] \quad (17b)$$

for the plasma-velocity vector \vec{u} . The nonvanishing components of the shear tensor in this case are

$$S_{11} = - 2(c/\mu)(\phi_c/a^2)(x^2 + 2y^2) x \quad (18a)$$

$$S_{22} = (c/\mu)(\phi_c/a^2)(3x^2 + 5y^2) x \quad (18b)$$

$$S_{33} = - (c/\mu)(\phi_c/a^2)(x^2 + y^2) x \quad (18c)$$

and

$$S_{12} = S_{21} = - (c/2\mu)(\phi_c/a^2)(3x^2 + 7y^2) y \quad (18d)$$

where $x = r \cos \phi$ and $y = r \sin \phi$ in the equatorial plane. The calculation of S_{33} in (18c) requires slightly devious methods, since it is not true that $\partial u_z / \partial z = 0$ in the equatorial plane. However, it follows from (17) and (15) that $(\partial u_x / \partial x) + (\partial u_y / \partial y) = (1/2) \nabla \cdot \vec{u}$, and therefore that $\partial u_z / \partial z = (1/2) \nabla \cdot \vec{u}$; this implies that $S_{33} = (1/6) \nabla \cdot \vec{u}$, and inspection of (18) reveals that the shear matrix is indeed traceless, as is required by (14). Note that (18) does not contain ϕ_r , the parameter associated with rigid rotation of the magnetosphere.

Of special interest in the present context is the quantity

$$s \equiv \sum_{ij} \hat{u}_i S_{ij} \hat{E}_j = \sum_{ij} \hat{E}_i S_{ij} \hat{u}_j \quad (19)$$

which represents the velocity shear measured with respect to a displacement normal to the velocity itself in the plane perpendicular to \vec{B} . The symbols \hat{E}_i and \hat{u}_j in (19) denote Cartesian components of the unit vectors parallel to \vec{E} and \vec{u} , respectively. Evaluation of (19) in the equatorial plane yields

$$\begin{aligned} s = & - [r^4 (13x^2 + 28y^2)y - 2(\phi_r a^3/\phi_c) r^2 (5x^2 + 14y^2) \\ & + 7 (\phi_r a^3/\phi_c)^2 y] r^2 (c\phi_c/2a^2 \mu) \\ & + [r^4 (x^2 + 4y^2) - 4(\phi_r a^3/\phi_c) r^2 y + (\phi_r a^3/\phi_c)^2] \end{aligned} \quad (20)$$

where $r^2 = x^2 + y^2$. Both numerator and denominator of (20) vanish at $y = (\phi_r a^3/\phi_c)^{1/3}$ on the dawn-dusk meridian ($x = 0$), but the expression for s remains continuous and approaches the value $-(7c/4\mu)\phi_r a$ there. This is the point at which equipotentials seem to cross in Fig. 7, and at which the plasma drift velocity therefore vanishes.

Contours of constant s in the xy plane are a measure of the direction along which striations will be approximately aligned. These are shown in Fig. 11, which is to be considered together with the equipotential contours from Fig. 8. The amount of shear thus seems to increase with r in the region of open equipotentials, and therefore in the region corresponding to the auroral zone. This means that the selection mechanism for \vec{k} becomes increasingly effective with increasing L , in accordance with the observational pattern (J. C. Siren, personal communication, 1982) illustrated in Figure 2. In other

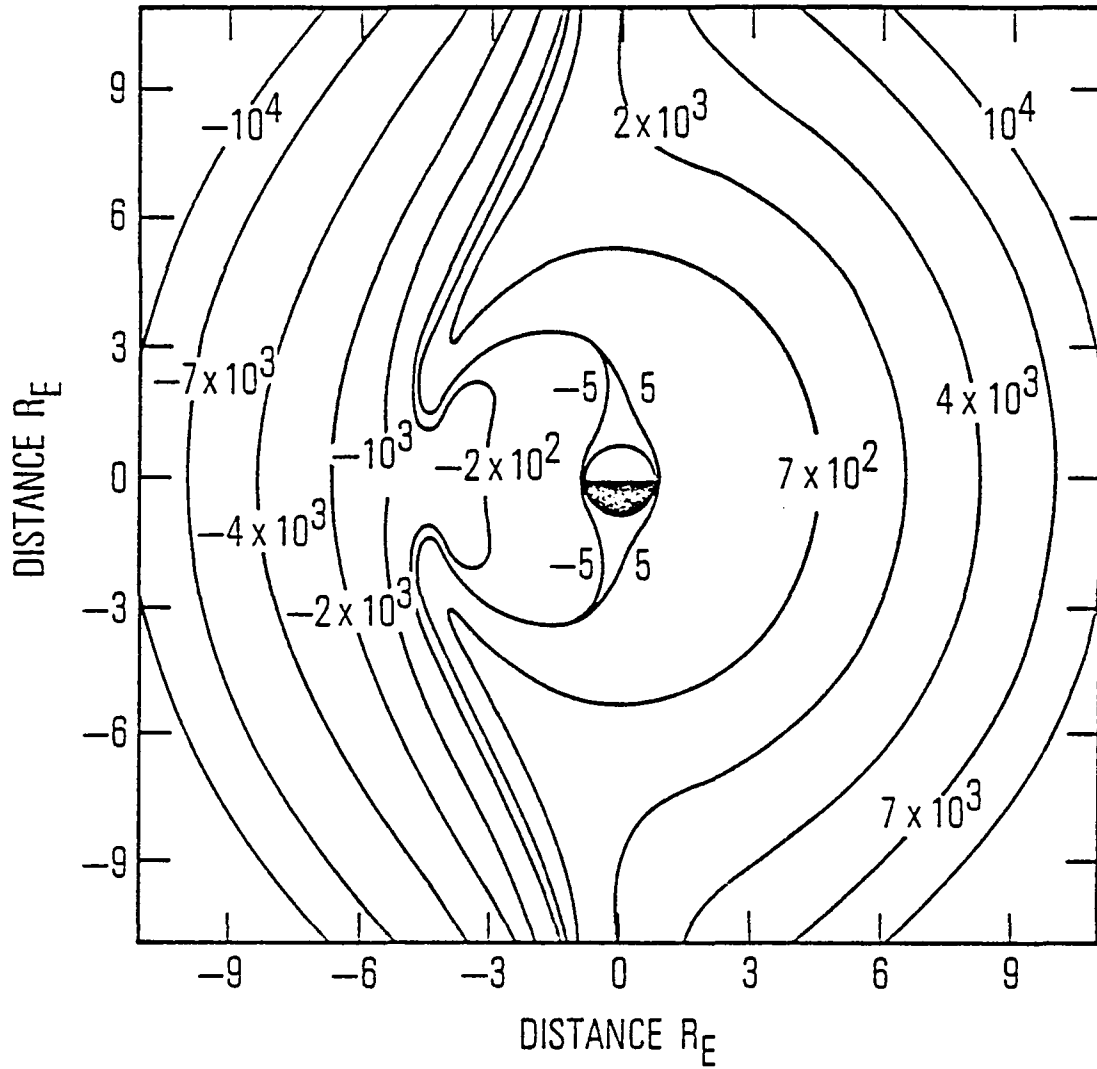


Fig. 11. Contours of constant shear s [defined in Eq. (19)] of the convection flow corresponding to the electric potential of Fig. 8.

words, the morningside portion of the diffuse aurora evolves into azimuthally elongated bands (suggesting a unique \vec{k}) at the higher L values but into a patchy morphology (suggesting a jumbled superposition of \vec{k} vectors) at the lower L values. Since the flow model described by (12) yields $s = (1/2)(du/dx)$, which is roughly appropriate on the local scale (as distinguished from the global scale of (20)), we presume that the "wave-normal" angle $\theta(t)$ and "wave vector" $\vec{k}(t)$ for the mirror instability will evolve roughly in accordance with the equations

$$\tan \theta(t) \equiv \vec{k} \cdot \hat{E}/\vec{k} \cdot \hat{u} = \tan \theta_0 + 2 \int_0^t s(t') dt' \quad (21a)$$

and

$$k_{\perp}(t) = \{1 + [\tan \theta_0 + 2 \int_0^t s(t') dt']^2\}^{1/2} |\vec{k} \cdot \hat{u}|_0 \quad (21b)$$

as one follows the $\vec{E} \times \vec{B}$ drift of a plasma element in more realistic flow geometries, such as that which leads to (13). The subscript 0 in (21) denotes evaluation at time $t = 0$.

We have so far neglected the effect of velocity shear on the plasma stability of the flow-velocity field itself. However, it is well known that velocity shear can lead to a Kelvin-Helmholtz instability whereby irregularities and eddies develop in the velocity field. Familiar examples of this from everyday experience include wind-driven surface waves on a body of water and flags waving in a steady breeze. The effect of Kelvin-Helmholtz instability on auroral forms was analyzed by Hallinan and Davis [1970]. Figure 2 contains clear evidence of this effect on the azimuthally elongated forms that evolve out of the diffuse aurora, as well as on the discrete arc.

One might question our use of a dipolar magnetic-field model in the outer magnetosphere, to which the auroral oval maps, for the purpose of calculating velocity shear. Indeed, it is not very difficult to calculate S_{ij} as a function of r , θ , and ϕ for a model magnetosphere like that shown in Fig. 1. Since our essential points concerning the selection of \vec{k} vector and its connection to morningside auroral morphology can be made with the simpler dipolar calculation, we shall not be involved with such a complex case.

VI. MODULATION OF CYCLOTRON INSTABILITY

The above results suggest that the mirror instability creates spatial irregularities in plasma density and magnetic-field strength in the equatorial portion of the outer magnetosphere, and that such irregularities are typically aligned with the plasma-convection pattern. We presume that such irregularities modulate the wave-particle interaction that is responsible for the diffuse auroral precipitation of energetic electrons. The precipitating electrons have perhaps tens of keV of energy and interact most probably with electrostatic electron-cyclotron waves, since the diffuse aurora occurs well outside the plasmasphere. The particles responsible for the mirror instability are mainly ions of the same energy range. In other words, the mirror instability modulates the electron-cyclotron instability, and altogether different particle populations are involved in the two instabilities.

We analyze the effects of this modulation on the intensity of electrostatic-cyclotron waves and on energetic-electron precipitation by means of the model equations introduced by Schulz [1974a] to simulate the Kennel-Petschek [1966] process. These equations are of the form

$$\frac{dI}{dt} = - \frac{\lambda I}{1 + \lambda \tau} + S \quad (22a)$$

and

$$\frac{1}{\lambda} \frac{d\lambda}{dt} = \frac{2 \gamma^* (I/I^*)}{1 + \gamma \tau} + |\vec{v}_g \cdot \hat{B}| \frac{\ln R}{La} + \frac{W}{\lambda} \quad (22b)$$

and they are designed to simulate the significant physical phenomena without

imposing the heavy calculational burden that an analysis from first principles would entail. The symbols λ and I in (22) correspond to wave and particle intensities, while the symbols W and S represent their respective source strengths. For our considerations here, we assume that all electrostatic cyclotron waves are generated by the energetic electrons of interest, so $W = 0$. The particle lifetime approaches the strong-diffusion lifetime τ (~ 100 sec) in the limit $\lambda\tau \gg 1$ and approaches $1/\lambda$ in the weak-diffusion limit $\lambda\tau \ll 1$. The growth rate for wave amplitude is represented as $(1 + \lambda\tau)^{-1} \gamma^* (I/I^*)$. The factor $(1 + \lambda\tau)^{-1}$ implicitly describes the dependence of the growth rate on pitch-angle anisotropy, which vanishes in the limit of strong diffusion ($\lambda\tau \gg 1$). The normalizing factor I^* for particle intensity is analogous to the intensity limit described by Kennel and Petschek [1966] in the context of unstable whistler-mode waves. The factor γ^* expresses the proportionality of growth rate to particle intensity at fixed anisotropy. The term $|\vec{v}_g \cdot \hat{B}/La| \ln R$ in (22b) describes the fact that waves have only a certain probability R of survival after propagating a distance $\sim La$ along the field line at group velocity \vec{v}_g , where L is the magnetic shell parameter and a is the radius of the earth. Thus, the parameter R serves as an effective internal-reflection coefficient for wave energy.

The time derivatives that appear in (22) must be interpreted as total (Lagrangian) time derivatives in the reference frames of the particles and waves, respectively. The difference between reference frames must be reconciled before (22a) and (22b) can be solved self-consistently. Thus, we must write

$$dI/dt = (\partial I/\partial t) + \vec{u} \cdot \nabla_{\perp} I + r\bar{\Omega}_3 \hat{\phi} \cdot \nabla_{\perp} I \quad (23a)$$

and

$$d\lambda/dt = (\partial\lambda/\partial t) + \vec{u} \cdot \nabla_{\perp} \lambda + \vec{v}_g \cdot \nabla_{\perp} \lambda \quad (23b)$$

where \vec{u} is the convection velocity $(c/B^2) \vec{E} \times \vec{B}$ and $r\bar{\Omega}_3 \hat{\phi}$ is the bounce-averaged gradient-curvature drift velocity (mapped to the equator) for the average energetic electron. The spatial derivatives in (23) involve ∇_{\perp} rather than ∇ because (22) represents (as usual) a bounce-averaged treatment of the wave-particle interaction.

We seek a steady-state solution of (22), a solution for which the important spatial variations of λ , I , and γ^*/I^* occur in the direction of the \vec{k} vector of the mirror instability, i.e., in the direction of the electric field \vec{E} . The tendency of strong shear in the convection velocity $\vec{u} = (c/B^2) \vec{E} \times \vec{B}$ to select this orientation for \vec{k} has been demonstrated above. We reduce the steady-state problem from two spatial dimensions to one by neglecting any variation of λ , I , or γ^*/I^* in the direction of \vec{u} , i.e., $\vec{u} \cdot \nabla_{\perp} = 0$. Thus, we sacrifice a description of global structure in order to concentrate on spatial modulations produced locally by the mirror instability. Thus, we can define a local Cartesian coordinate system (κ, μ) such that the unit vectors $\hat{\kappa}$ and $\hat{\mu}$ are parallel to \vec{k} and \vec{u} respectively. In this system, $\nabla_{\perp} = \hat{\kappa} \frac{\partial}{\partial \kappa}$ and the furrows of the mirror instability lie parallel to $\hat{\mu}$, as illustrated in Fig. 12. Note the important difference between the gradient drift direction $\hat{\phi}$ and the local vectors $(\hat{\kappa}, \hat{\mu})$ oriented by the shear action in the convection flow.

A further notational simplification of (22) can be introduced by normalizing to the weakly diffusive ($\lambda\tau \ll 1$), unmodulated Kennel-Petschek limit without residual wave source ($W = 0$), i.e., $I \equiv I_0^*$, $\gamma \equiv \gamma_0^*$ and $d\lambda/dt =$

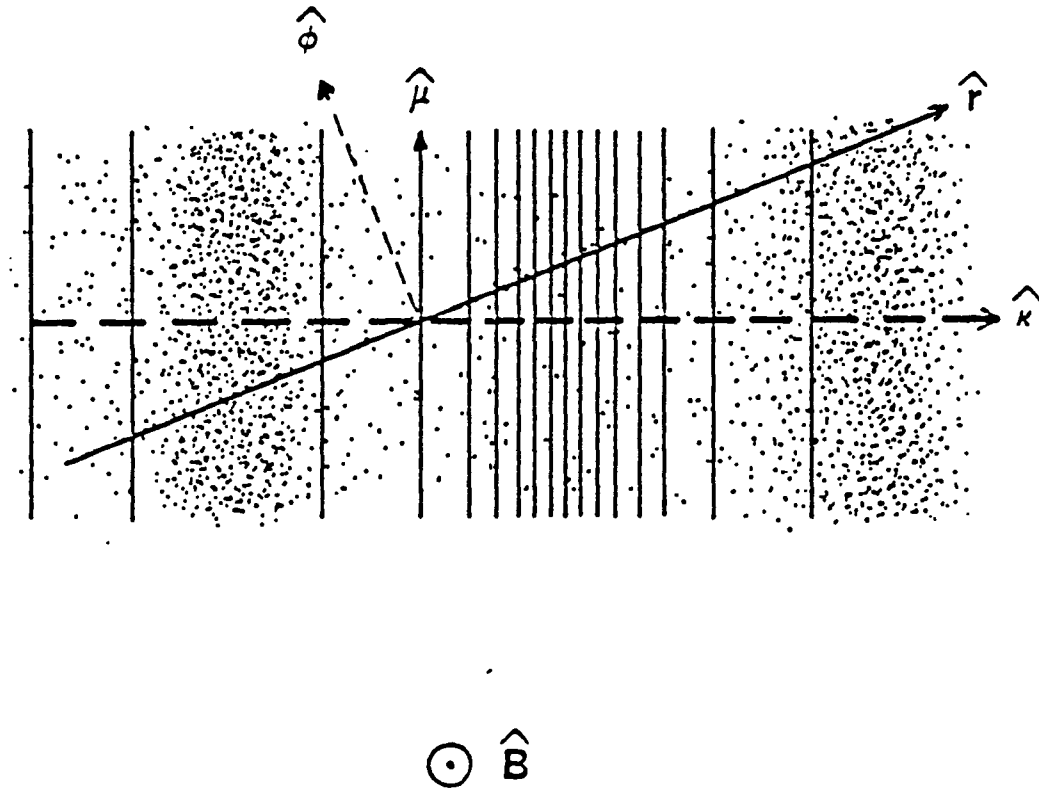


Fig. 12. Coordinate system used in considering electron flux modulation. $\hat{\phi}$ is the azimuthal direction, \hat{k} is the wave vector direction, and $\hat{\mu}$ is the convection flow direction.

0. In this limit (22b) yields

$$2\gamma_0^* = - |\vec{v}_g \cdot \hat{B}| \frac{\ln R}{L a} \quad (24)$$

which can be reintroduced in (22b) to eliminate the constants involved. Further simplification can be achieved if I and γ are to be measured in units of I_0^* and γ_0^* .

Under these assumptions, the model equations become, in the frame of the flux tube drifting with velocity \vec{u} ,

$$\tau r \bar{n}_3 (\hat{\phi} \cdot \hat{\kappa}) \frac{\partial(I/I_0^*)}{\partial \kappa} = - \frac{\lambda \tau (I/I_0^*)}{1 + \lambda \tau} + (\tau S/I_0^*) \quad (25a)$$

$$\frac{1}{\lambda} (\vec{v}_g \cdot \hat{\kappa}) \frac{\partial(\lambda \tau)}{\partial \kappa} = \frac{2 \gamma^* \tau (I/I_0^*)}{1 + \lambda \tau} - 2\gamma_0^* \tau \quad (25b)$$

where the source S and strong-diffusion lifetime τ are regarded as constants. The periodic spatial variability of interest originates in the ratio (γ^*/I^*) in (25b), which we model as a plane wave modulation of the unmodulated Kennel-Petschek limit (γ_0^*/I_0^*)

$$\gamma^*/I^* = (\gamma_0^*/I_0^*) \exp(Q \sin k \kappa) \quad (26)$$

We expect the parameter Q in (26) to be of order unity. This estimate is based on the expectation that the mirror instability should modulate various plasma parameters (e.g., density, temperature, and magnetic field strength) by about $\pm 10\%$, whereas the resonant-particle energy exceeds the electron temperature by a factor ~ 10 . The amplitude Q of the argument of the exponential function in (26) should amount roughly to the product of these two dimension-

less factors in the case of a resonant-particle instability, thus $Q \sim 1$.

In order to proceed with the analysis of the model, we need to determine the group velocity of the electrostatic cyclotron waves \vec{v}_g in the frame of the drifting flux tube. As far as we are able to determine, observation does not shed any light on this point, but, considering the spectrum of particle drift velocities involved, \vec{v}_g is probably bounded by $\vec{v}_g = 0$ (waves drifting with the cold plasma in the flux tube) on the one hand and by $\vec{v}_g = r\bar{\Omega}_3 \hat{\phi}$ (waves drifting with the energetic electrons) on the other. We shall investigate both limits to show that the spatial modulation is effective in both cases.

Model A: Waves drifting with energetic electrons ($\vec{v}_g = r\bar{\Omega}_3 \hat{\phi}$). Defining the dimensionless variable $\xi \equiv \kappa/\tau r\bar{\Omega}_3(\hat{\phi} \cdot \hat{\kappa})$, the model equations for this case can be written in dimensionless form.

$$\partial \bar{I}/\partial \xi = -\frac{\bar{\lambda} \bar{I}}{1 + \bar{\lambda}} + \bar{S} \quad (27a)$$

$$\partial (\ln \bar{\lambda})/\partial \xi = (2 \gamma_0^* \tau) \left[\frac{\bar{I}}{1 + \bar{\lambda}} \exp(Q \sin \bar{k} \xi) - 1 \right] \quad (27b)$$

where $\bar{\lambda} = \lambda \tau$, $\bar{I} = I/I_0^*$, $\bar{S} = \tau S/I_0^*$ and $\bar{k} = k \tau r\bar{\Omega}_3(\hat{\phi} \cdot \hat{\kappa})$. Numerical solution of (27) as a nonlinear initial value problem is implemented. The numerical steady state exhibits spatial modulation of the trapped electron flux \bar{I} , but, more importantly, very deep spatial modulations of the precipitation flux $\bar{\lambda} \bar{I}/(1 + \bar{\lambda})$ is found. Figure 13 shows the solutions for a case with typical parameters: $\bar{S} = 0.1$, $Q = 1.0$, $\bar{k} = 3.0$ and $2\gamma_0^* \tau = 30.0$. The scale length of the spatial modulation (furrows) for this case is $\kappa_0 = (2\pi/\bar{k})[\tau r\bar{\Omega}_3(\hat{\phi} \cdot \hat{\kappa})]$.

Model B: Waves drifting with cold plasma ($\vec{v}_g = 0$). We obtain for this case

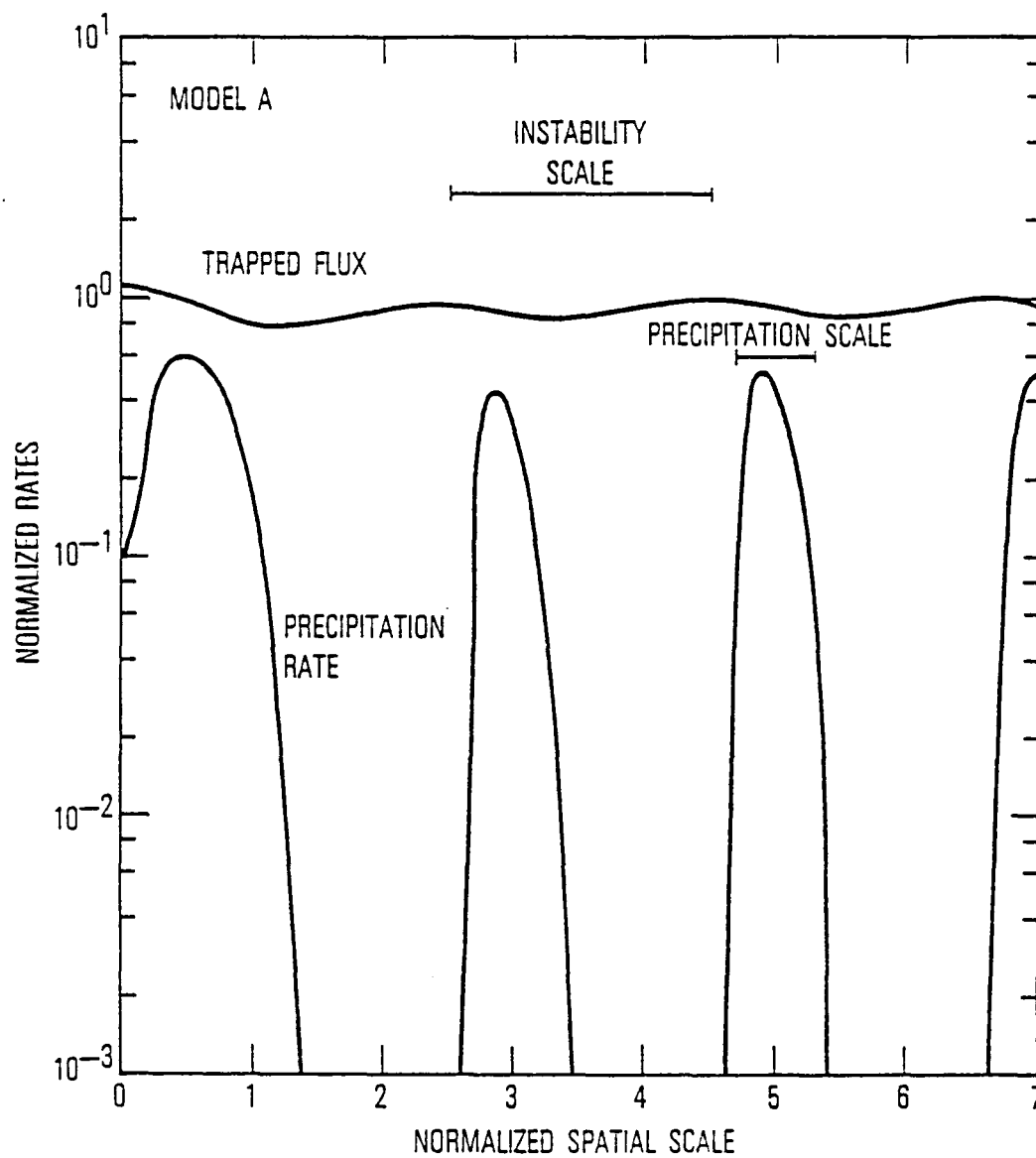


Fig. 13. Electron flux modulation by mirror instability for the case in which electrostatic cyclotron waves drift with energetic electrons (Model A).

$$\partial \bar{I} / \partial \xi = - \frac{\bar{\lambda} \bar{I}}{1 + \bar{\lambda}} + \bar{S} \quad (28a)$$

$$1 + \bar{\lambda} = \bar{I} \exp(Q \sin \bar{k} \xi) \quad (28b)$$

The algebraic equation (28b) can be solved for $\bar{\lambda}$. Because the diffusion rate $\bar{\lambda}$ is restricted to positive or zero values, we have

$$\bar{\lambda} = \text{Max} [\bar{I} \exp (Q \sin \bar{k} \xi) - 1; 0] \quad (29)$$

whence

$$\frac{\partial \bar{I}}{\partial \xi} = \bar{S} - \text{Max} [\bar{I} - \exp(-Q \sin \bar{k} \xi); 0] \quad (30)$$

Equation (30) can be solved numerically in the same way as (27). For the same parameter values given in Model A, above, the solution of (30) is shown in Fig. 14. The properties and the scaling of this solution is the same as that of Fig. 13 except that, as the result of (29), the precipitation rate at minimum is exactly zero. The solution to (30) relaxes to the steady state at a rate slower than that of (27); however, this is not of any significance since only the steady rate is to be considered in the context of our theory.

With regard to (30), it is interesting to note that one can seek an analytic solution by an expansion of the form

$$\bar{I} = \bar{S} + I_0(Q) + \sum_{n=1}^{\infty} [C_n \cos n\bar{k}\xi + S_n \sin n\bar{k}\xi] \quad (31)$$

by taking advantage of the expansion [e.g. Olver, 1964; p. 376]

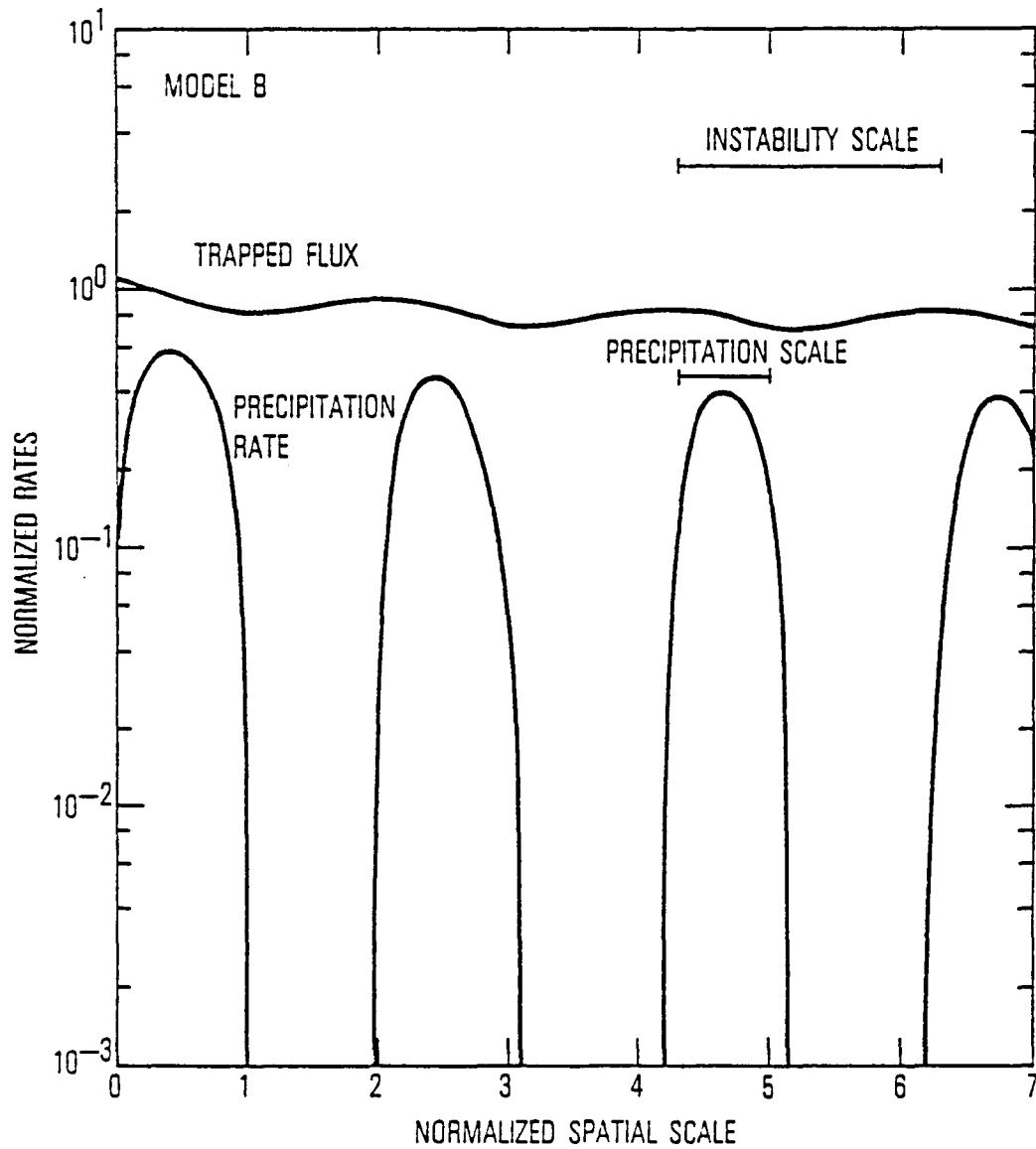


Fig. 14. Electron flux modulation by mirror instability for the case in which electrostatic cyclotron waves drift with cold plasma (Model B).

$$\begin{aligned} \exp(-Q \sin \bar{k}\xi) &= I_0(Q) + 2 \sum_{q=1}^{\infty} (-1)^q I_{2q}(Q) \cos(2q\bar{k}\xi) \\ &- 2 \sum_{q=0}^{\infty} (-1)^q I_{2q+1}(Q) \sin(2q\bar{k}\xi + \bar{k}\xi) \end{aligned} \quad (32)$$

The results of this exercise confirm the properties of the numerical solution.

In both models, the scale length of the modulation is

$$\kappa_0 = |(2\pi/\bar{k})[\tau \bar{\Omega}_3 (\hat{\phi} \cdot \hat{\kappa})]| = 2\pi/k \quad (33)$$

To compare κ_0 with the ion gyroradius scale of a typical 3-keV proton $\rho_0 \sim L^3$ km, we note that $\bar{\Omega}_3 \tau \sim 10^{-6} L^5$ [e.g., Schulz and Lanzerotti, 1974; p. 21; Schulz, 1974b]. The angle $\hat{\kappa} \cdot \hat{\phi}$ can be obtained from (1) by requiring that $\hat{\kappa} = \pm \hat{E}$ for reasons documented above. Thus we obtain

$$\begin{aligned} |(\tau/\rho_0)(\hat{\kappa} \cdot \hat{\phi}) \bar{\Omega}_3 \tau| &\sim 10^{-2} L^6 [L^6(1 + 3 \sin^2 \phi) \\ &- 2(\phi_r/\phi_c) L^3 \sin \phi + (\phi_r/\phi_c)^2]^{-1/2} \cos \phi \end{aligned} \quad (34)$$

For auroral conditions, $L^3 \gg (\phi_r/\phi_c)$, so (34) implies

$$\tau \bar{\Omega}_3 (\hat{\kappa} \cdot \hat{\phi}) \sim 10^{-2} \rho_0 L^3 \cos \phi \sim 10^{-2} L^6 \cos \phi \quad \text{km} \quad (35)$$

Using the assumed values $\bar{k} = 3$ and $L = 7$, (33) and (35) imply that the value of κ_0 mapped to the ionosphere is about 6 km. This is roughly in agreement with the observed scale modulation of morningside diffusive auroras [Akasofu, 1974] and with patches [Yamamoto and Oguti, 1982]. Further confirmation of

spatial modulation at the ~ 10 km scale has recently been obtained [Vondrak et al., 1983] by incoherent-scatter radar observations. These were taken equatorward of the diffuse aurora in the evening sector. Although our theory prefers modulation in the morning sector because of the observed pattern of ion pitch-angle anisotropies obtained by SCATHA, all other elements of the theory can be operative at any local time provided that the mirror instability can be driven.

Finally we make a fairly obvious point related to the time dependence of (23), which we ignored in the subsequent development but need not be in general. In general, the colder convecting plasma can establish the spatial modulation of the magnetic field in the manner considered prior to this section. The source of the hot electrons, which precipitate and drive the aurora, need not be time-independent. Indeed, auroral brightenings associated with injection events would imply that the source of hot electrons is definitely time-dependent. If so, the mechanisms of spatial modulation can be translated into both time and space modulations, as required by (23). The natural consequence would be a theory of morningside pulsating patches and diffuse auroral striations [e.g. Berkey, 1980] (as distinguished from the theory of the rare pulsating arcs [Cornwall and Chiu, 1982]). The oscillatory time-dependent structure of (22), in isolation from the spatial modulation of the colder plasma by the mirror instability, has been treated by Davidson [1979] who considered a single component of electrons only and, thus, is not able to account for the spatial structures and their drifts. According to our theoretical mechanism, including time-dependence, pulsating structures (striations and patches) would prefer the morningside and, more importantly, would not necessarily be associated with micropulsations. Obviously, pulsating auroras have local as well as global morphologies [Royrvik and Davis, 1977].

Our observations here are to be taken in the context of a new avenue of thought on morningside pulsating auroras, not a global model as yet. However, salient observed features such as recurrent patterns [Oguti, 1976] are easily understood in terms of quasi-periodic injections of hot electrons which drift over and are caused to precipitate by slowly varying spatial patterns of furrows set-up by the warm plasma convection.

VII. CONCLUSIONS

In the above we have constructed a theoretical framework which links together diverse observations such as the local time structure of plasma characteristics, the global structure of magnetospheric convection, and the mechanisms of wave-particle interactions into a coherent picture which offers a possible explanation of the morphology of the aurora in the post-midnight and morning sectors. This picture complements, indeed demands, the existence of upward ionospheric ion acceleration in the evening discrete arc. Thus, in a real sense, it embodies the important principle that the aurora arises as result of electrodynamic coupling between the magnetosphere and the ionosphere.

Basing our theory upon observations of auroral and subauroral distribution functions by the SCATHA satellite near the equatorial plane, we offer kinetic explanations of the morningside auroral morphology. We argue that zero frequency mirror instability can be driven by warm ions convected in from the plasmasheet and that the instability is stabilized on the eveningside by field-aligned ions from the discrete arc. We further argue that these spatial modulations of the magnetic field and warm plasma density can modulate the precipitation rates of hot electrons according to a morphology selected by the action of shear in the convecting warm plasma flow. An essential ingredient of our theory is the different actions of the warm and hot plasmas, accounting for the observation that morningside auroral structures drift with the warm convecting plasma but not with the hot electrons that produce the aurora itself. In the present state, our theory represents an assembly of coherently related theoretical and observational segments; as such, it is not yet a numerical model. A numerical model will be constructed in the future in the

context of global arc formation theory integrating the present work with work on the evening aurora [e.g. Chiu et al., 1981].

References

- Akasofu, S. -I., Discrete, continuous and diffusive auroras, Planet. Space Sci., 22, 1723, 1974.
- Akasofu, S. -I., Recent progress in studies of DMSP auroral photographs, Space Sci. Rev., 19, 169, 1976.
- Akasofu, S. -I., Auroral arcs and auroral potential structure, in Physics of Auroral Arc Formation, ed. S. -I. Akasofu and J. R. Kan, p. 1, AGU Monograph 25, AGU, Washington, D.C., 1981.
- Akasofu, S. -I. and J. R. Kan, Dayside and nightside auroral arc systems, Geophys. Res. Lett., 7, 753, 1980.
- Berkey, F. T., Temporal fluctuations in the luminosity of diffuse auroras, J. Geophys. Res., 85, 6075, 1980.
- Chen, A. J., Penetration of low-energy protons deep into the magnetosphere, J. Geophys. Res., 75, 2458, 1970.
- Chiu, Y. T., Self-consistent electrostatic field mapping in the high-latitude ionosphere, J. Geophys. Res., 79, 2790, 1974.
- Chiu, Y. T. and J. M. Cornwall, Electrostatic model of a quiet auroral arc, J. Geophys. Res., 85, 543, 1980.
- Chiu, Y. T., J. M. Cornwall and M. Schulz, Auroral magnetosphere-ionosphere coupling: A brief topical review, Solar-Terrestrial Predictions Proceedings, Vol. II, p. 494, NOAA, Boulder, Colorado, 1979.
- Chiu, Y. T., J. M. Cornwall and M. Schulz, Effects of auroral-particle anisotropies and mirror forces on high-latitude electric fields, in Physics of Auroral Arc Formation, ed. S. -I. Akasofu and J. R. Kan, p. 234, AGU Monograph 25, AGU, Washington, D.C., 1981.

- Chiu, Y. T., A. L. Newman and J. M. Cornwall, On the structure and mapping of auroral electrostatic potentials, J. Geophys. Res., 86, 10029, 1981.
- Chiu, Y. T., J. M. Cornwall, J. F. Fennell, D. J. Gorney and P. F. Mizera, Auroral plasmas in the evening sector: Satellite observations and theoretical interpretations, Space Sci. Rev., in press, 1982.
- Chiu, Y. T. and A. M. Kishi, Theory of time-dependent auroral plasma injection, J. Geophys. Res., in preparation, 1983.
- Cornwall, J. M. and Y. T. Chiu, Ion distribution effects of turbulence on a kinetic auroral arc model, J. Geophys. Res., 87, 1517, 1982.
- Coroniti, F. V. and C. F. Kennel, Electron precipitation pulsations, J. Geophys. Res., 75, 1279, 1970.
- Cowley, S. W. H. and M. Ashour-Abdalla, Adiabatic plasma convection in a dipole field: Variation of plasma bulk parameters with L, Planet. Space Sci., 23, 1527, 1975.
- Davidson, G. T., Self-modulated VLF wave-electron interaction in the magnetosphere: A cause of auroral pulsation, J. Geophys. Res., 84, 6517, 1979.
- Fennell, J. F., D. J. Gorney and P. F. Mizera, Auroral particle distribution functions and their relationship to inverted-V's and auroral arcs, in Physics of Auroral Arc Formation, ed. S. -I. Akasofu and J. R. Kan, AGU Monograph 25, p. 91, AGU, Washington, D.C., 1981.
- Fennell, J. F., D. R. Croley, Jr. and S. M. Kaye, Low-energy ion pitch angle distributions in the outer magnetosphere: Ion zipper distributions, J. Geophys. Res., 86, 3375, 1981.
- Frank, L. A., R. L. McPherron, R. J. DeCoster, B. G. Burek, K. L. Ackerson and C. T. Russell, Field-aligned currents in the earth's magnetotail, J. Geophys. Res., 86, 687, 1981.

- Gorney, D. J., A. Clarke, D. R. Croley, J. F. Fennell, J. G. Luhmann and P. F. Mizera, The distribution of ion beams and conics below 8000 km, J. Geophys. Res., 86, 83, 1981.
- Hallinan, T. J. and T. N. Davis, Small scale auroral arc distortions, Planet. Space Sci., 18, 1735-1744, 1970.
- Hasegawa, A., Drift mirror instability in the magnetosphere, Phys. Fluids, 12, 2642, 1969.
- Hasegawa, A., Plasma Instabilities and Non-linear Effects, Springer, Heidelberg, 217 pp., Germany, 1975.
- Hoffman, R. A. and C. S. Lin, Study of inverted-V auroral precipitation events, in Physics of Auroral Arc Formation, ed. S. -I. Akasofu and J. R. Kan, AGU Monograph 25, AGU, Washington, D.C., 1981.
- Johnstone, A. D., Pulsating auroras, Nature, 274, 119, 1978.
- Kaye, S. M., M. G. Kivelson and D. J. Southwood, Evolution of ion cyclotron instability in the plasma convection system of the magnetosphere, J. Geophys. Res., 84, 6397, 1979.
- Kaye, S. M., E. G. Shelley, R. D. Sharp and R. G. Johnson, Ion composition of zipper events, J. Geophys. Res., 86, 3383, 1981.
- Kennel, C. F. and H. E. Petschek, Limit on stably trapped particle fluxes, J. Geophys. Res., 71, 1-28, 1966.
- Kivelson, M. G. and D. J. Southwood, Approximations for the study of drift boundaries in the magnetosphere, J. Geophys. Res., 80, 3528, 1975.
- Kivelson, M. G., S. M. Kaye and D. J. Southwood, The physics of plasma injection events, in Dynamics of the Magnetosphere, ed. S. -I. Akasofu, Reidel, Dordrecht-Holland, p. 385, 1979.
- Lanzerotti, L. J., A. Hasegawa and C. G. MacLennan, Drift mirror instability in the magnetosphere: Particle and field oscillations and electron heating, J. Geophys. Res., 74, 5565, 1969.

- Lyons, L. R., Generation of large-scale regions of auroral currents, electric potentials, and precipitation by the divergence of the convection electric field, J. Geophys. Res., 85, 17, 1980.
- Lyons, L. R., Formation of discrete auroral currents and potentials, J. Geophys. Res., 86, 1, 1981.
- Mizera, P. F. and J. F. Fennell, Signatures of electric fields from high and low altitude particle distributions, Geophys. Res. Lett., 4, 311, 1977.
- Mizera, P. F., D. R. Croley, Jr. and J. F. Fennell, Electron pitch-angle distributions in an inverted-V structure, Geophys. Res. Lett., 3, 149, 1976.
- Morse, P. M. and K. U. Ingard, Theoretical Acoustics, 927 pp., McGraw-Hill, New York, 1968.
- Mozer, F. S., C. A. Cattell, M. K. Hudson, R. L. Lysak, M. Temerin and R. B. Torbert, Satellite measurements and theories of low-altitude auroral particle acceleration, Space Sci. Rev., 27, 155, 1980.
- Oguti, T., Recurrent auroral patterns, J. Geophys. Res., 81, 1782, 1976.
- Oguti, T., Television observations of auroral arcs, in Physics of Auroral Arc Formation, ed. S. -I. Akasofu and J. R. Kan, p. 31, AGU Monograph 25, AGU, Washington, D.C., 1981.
- Olver, F. W. J., Bessel functions of integer order, in Handbook of Mathematical Functions with Formulas, Graphs and Mathematical Tables, ed. M. Abramowitz and I. A. Stegun, pp. 355-433, U. S. Dept. of Commerce, National Bureau of Standards, Washington, D.C., 1966.
- Panofsky, W. K. H. and M. Phillips, Classical Electricity and Magnetism, 494 pp., Addison-Wesley, Reading, Mass., 1962.
- Richardson, J. D., J. F. Fennell and D. R. Croley, Jr., Observations of field-aligned ion and electron beams from SCATHA (P78-2), J. Geophys. Res., 86, 10015, 1981.

- Royrvik, O. and T. N. Davis, Pulsating aurora: Local and global morphology, J. Geophys. Res., 82, 4720, 1977.
- Scarf, F. L., J. H. Wolfe and R. W. Silva, A plasma instability associated with thermal anisotropies in the solar wind, J. Geophys. Res., 72, 933, 1967.
- Schulz, M., Particle saturation of the outer zone: A nonlinear model, Astrophys. Space Sci., 29, 233-242, 1974a.
- Schulz, M., Particle lifetimes in strong diffusion, Astrophys. Space Sci., 31, 37-42, 1974b.
- Schulz, M. and L. J. Lanzerotti, Particle Diffusion in the Radiation Belts, 215 pp., Springer-Verlag, New York, 1974.
- Schulz, M. and H. C. Koons, Thermalization of colliding ion streams beyond the plasmopause, J. Geophys. Res., 77, 248, 1972.
- Schulz, M., Y. T. Chiu and J. M. Cornwall, Theory of the auroral magnetosphere, Aeronomica Acta, No. 237, Institute D'Aeronomie Spatiale, Brussels, 1981.
- Southwood, D. J. and M. G. Kivelson, An approximate analytical description of plasma bulk parameters and pitch angle anisotropy under adiabatic flow in a dipolar magnetic field, J. Geophys. Res., 80, 2069, 1975.
- Volland, H., Models of global electric fields within the magnetosphere, Ann. Geophys., 31, 159, 1975.
- Vondrak, R. R., J. S. Murphree, C. D. Auger and D. D. Wallis, Ionospheric characteristics of a detached arc in the evening-sector trough, Geophys. Res. Lett., submitted, 1982.
- Wolfe, R. A., Effects of ionospheric conductivity on convective flow of plasma in the magnetosphere, J. Geophys. Res., 75, 4677, 1970.
- Yamamoto, T. and T. Oguti, Recurrent fast motion of pulsating auroral patches

1. A case study on optical and quantitative characteristics during a slightly active period, J. Geophys. Res., 87, 7603, 1982.

End of Document